frontiers | Frontiers in Marine Science

TYPE Original Research
PUBLISHED 12 June 2024
DOI 10.3389/fmars.2024.1418716

OPEN ACCESS

EDITED BY
Paraskevi Polymenakou,
Hellenic Centre for Marine Research (HCMR), Greece

REVIEWED BY
Giovanni Martinelli,
National Institute of Geophysics and Volcanology, Italy
Zhifeng Wan,
Sun Yat-sen University, China

*CORRESPONDENCE
Wei Zhang
zwgmgs@foxmail.com
Pibo Su
spb_525@sina.com

RECEIVED 17 April 2024
ACCEPTED 22 May 2024
PUBLISHED 12 June 2024

CITATION
Zhang W, Liang J, Su P, Meng M, Huang W, Liu P, Yuan S and Ji C (2024) Dynamic accumulation of a high-grade gas hydrate system: insights from the trial production gas hydrate reservoir in the Shenhu area, northern South China Sea.
Front. Mar. Sci. 11:1418716.
doi: 10.3389/fmars.2024.1418716

Dynamic accumulation of a high-grade gas hydrate system: insights from the trial production gas hydrate reservoir in the Shenhu area, northern South China Sea

Wei Zhang[1,2,3]*, Jinqiang Liang[1,2,3,4], Pibo Su[1,2,3]*, Miaomiao Meng[2,3,4], Wei Huang[2,3,4], Pengqi Liu[1,3], Sheng Yuan[1,3] and Chunsheng Ji[1,3]

[1]Sanya Institute of South China Sea Geology, Guangzhou Marine Geological Survey, China Geological Survey, Sanya, China, [2]National Engineering Research Center of Gas Hydrate Exploration and Development, Guangzhou, China, [3]Academy of South China Sea Geological Science, China Geological Survey, Sanya, China, [4]Gas Hydrate Engineering and Technology Center, China Geological Survey, Guangzhou, China

The ultimate enrichment level and quantity of gas hydrate resources are influenced by the dynamic process of accumulation and preservation. High-resolution 3-D seismic data, logging while drilling (LWD), pressured coring, and *in situ* testing were used to characterize the dynamic accumulation and preservation of the trial production high-grade gas hydrate reservoir (HGGHR) in the Shenhu area. Through seismic variance analysis and ant-tracking, we found that newly identified mud diapir-associated faults with three development stages controlled the migration and accumulation of gas hydrate and shifted the base of the gas hydrate stability zone (BGHSZ), resulting in dynamic accumulation and dissociation of gas hydrates. The recognized double bottom simulating reflectors (BSRs) were concluded to have been formed due to the shift of the BGHSZ caused by the variational equilibrium conditions. The interval between the double BSRs was inferred to be a disequilibrium zone where gas recycling occurred, contributing to the coexistence of gas hydrates and free gas and the dynamic formation of the HGGHR. Multiple gliding faults formed within the GHSZ in the late period have altered the HGGHR and control the present thickness and distribution of the gas hydrates and free gas in the hanging wall and footwall. Under the influence of geothermal fluids and the fault system associated with the mud diapir, the HGGHR experienced dynamic accumulation with three stages, including early accumulation, medium-term adjustment, and late alteration and preservation. We conclude that four factors affected the formation, distribution, and occurrence of the HGGHR: the geothermal fluids accompanying the deep mud diapir below the reservoir, the dual supply of thermogenic gas and biogenic

gas, the recycling of hydrate gas beneath the BGHSZ, and the post-gas hydrate faults developed within the GHSZ. A geological model illustrating the dynamic formation of the trial production HGGHR was proposed, providing a reference for future exploration of HGGHRs with a great production potential in deepwater settings.

KEYWORDS

Hydrate recycling, dynamic accumulation mechanism, mud diapir associated fault, coexistence of hydrate and free gas, hydrate preservation, trial production, Shenhu area, South China Sea

1 Introduction

Natural gas hydrates (hereinafter gas hydrates), characterized by a wide distribution, abundant resources, and high energy density, play a vital role in global energy resources and are considered a potential alternative energy source to supplement or replace conventional fossil energies in the future (Collett, 2000; Boswell and Collett, 2006; Makogon et al., 2007). Therefore, the formation and accumulation mechanisms of gas hydrates and their exploration and development are a major scientific issue of concern to scientists and engineers around the world (Collett et al., 2009; Dallimore and Collett, 2005; Collett et al., 2011; Fujii et al., 2015; Kim et al., 2015; Jang et al., 2019; Liang et al., 2019). Gas hydrates have been discovered at more than 230 sites through drilling and sampling in onshore and offshore areas, as well as in permafrost regions, and gas hydrate reservoirs with good exploitation potential have been confirmed in several places, including North America, the Nankai Trough, the Indian offshore area, and the South China Sea (SCS) (Collett et al., 2009; Li et al., 2018; Collett et al., 2019; Shukla et al., 2019; Yamamoto et al., 2019; Ye et al., 2020). Gas hydrates production trials have been implemented in several regions, including the Mackenzie Permafrost, Canada (Bybee, 2004; Collett, 2005; Dallimore and Collett, 2005), the Nankai Trough, Japan (Fujii et al., 2015; Konno et al., 2017; Yamamoto et al., 2019), and the Shenhu area in the northern SCS (Li et al., 2018; Ye et al., 2020; Liu and Li, 2021). These gas hydrate production tests have made significant progress and have proven that gas hydrates can be exploited safely and controllably to a certain extent under the present technological conditions. With the fast-growing global demand for energy, it is of great significance to master the accumulation theory and technology of commercial exploration and development of gas hydrates in order to alleviate the energy crisis and to promote environmentally friendly and sustainable development around the world. However, the exploration of gas hydrate accumulations suitable for long-term trail production or commercial development remains a challenging task. Therefore, it is necessary to explore and understand the formation and accumulation mechanisms of hydrate reservoirs that are preferred for trial production or commercial exploitation. The majority of studies on gas hydrate accumulation have focused on the static characterization of a gas hydrate system, including the gas hydrate stability zone (GHSZ), reservoir, gas source, and migration pathways (Collett, 2009); however, the complete formation process of a gas hydrate system, especially the geological effects of the internal structural features of the gas hydrate reservoir and underlying the base of the gas hydrate stability zone (BGHSZ) on the gas hydrate accumulations, lack sufficient study. In recent years, scientists have begun to pay close attention to the dynamic accumulation of gas hydrate systems. Multiple bottom simulating reflectors (BSRs), transient response of the GHSZ, and the apparent disequilibrium of gas hydrate accumulations has reported in Gulf of Mexico (Portnov et al., 2023), offshore areas in the Tumbes Basin, Peru (Auguy et al., 2017), in the Danube Fan, Black Sea (Hillman et al., 2018a; Riedel et al., 2021), and in the northern Hikurangi margin (Han et al., 2021). Submarine gas plumes, cold seeps, and carbonate rocks related to gas hydrate decomposition also indicate that a gas hydrate system may have a dynamic accumulation, decomposition, and re-accumulation processes (Bohrmann et al., 1998), which directly determine the hydrate reserves and the economic evaluation of the exploitation of the system in the future. Gas hydrate accumulation depends on the temperature, pressure, and other conditions, and a change in the GHSZ will cause the dynamic accumulation and dissociation of gas hydrates. Theoretically, sea-level variations, climate change, tectonic deformation, deposition and erosion, and gas source changes will alter the GHSZ, causing a shift in the BGHSZ and leading to the decomposition of gas hydrates and the escape of the released gas (Bünz et al., 2003; Auguy et al., 2017; Zander et al., 2017). When equilibrium conditions are reached again, the hydrates can reprecipitation and may exhibit a multilayer distribution (Zander et al., 2017; Zhang and Wright, 2017; Kunath et al., 2020; Zhang et al., 2020a). However, the process and controlling factors of the dynamic multistage accumulation of gas hydrates have not been fully revealed. In addition, a variety of geological processes have a destructive effect on hydrate accumulation, resulting in hydrate decomposition and a decrease in reserves. Apart from differences in the gas supply, migration pathways, and reservoir quality, differences in the preservation conditions are likely to cause the heterogeneous accumulation of gas hydrates (Boswell et al., 2019). The differences in hydrate saturation and thickness under the same tectonic and sedimentary background may also be caused by differences in the late preservation (Hillman et al., 2018b). Therefore, preservation

conditions may be the key to the occurrence and distribution of high-grade gas hydrate reservoirs characterized by high saturation, massive thickness and extensive coverage.

China is a country rich in gas hydrate resources, which are accumulated in the northwestern permafrost region and the area offshore of southern China (Wu et al., 2010; Lu et al., 2013; Wang et al., 2018). During more than two decades of investigation and exploration, China has carried out eight gas hydrate scientific drilling expeditions (GMGS1–GMGS8) in the SCS; recovered high saturation gas hydrate samples with multiple occurrences in the Shenhu sea, the Dongsha area, and the Qiongdongnan area; and confirmed the existence of gas hydrate reservoirs containing more than 200 billion cubic meters of natural gas resources (Wang et al., 2014; Zhang et al., 2015; Yang S. et al., 2017; Yang S. X. et al., 2017; Liang et al., 2019; Zhang et al., 2020b). In recent years, the China Geological Survey has successfully carried out two gas hydrate trial productions in the deep-water Shenhu area (Figure 1) and has made great breakthroughs in offshore gas hydrate exploration and development (Li et al., 2018; Ye et al., 2020).

The trial production target in the Shenhu area is a high-grade gas hydrate reservoir (HGGHR) characterized by a high saturation (~50%), large thickness (>10 m single layer thickness) and great hydrate reserve potential (Zhang et al., 2017; Qin et al., 2020). Although two successful gas hydrate mining tests have been implemented, the characteristics and controlling factors of the accumulation of this HGGHR are not yet fully understood. Why this HGGHR could form and accumulate in the clay-dominated sediments remains unclear. Previous studies have indicated that the dynamic accumulation of a gas hydrate system may have occurred in the Shenhu area, as evidenced by migrated submarine channel-levee systems where gas hydrates differentially precipitated (Zhang et al., 2020a), venting hydrate systems identified from seismic profiles (Liang et al., 2021), paleo-cold seeps indicated by authigenic carbonates and pore water anomalies (Lin et al., 2016; Deng et al., 2020; Hu et al., 2020; Zhang et al., 2022), and the coexistence of gas hydrates and free gas (Qian et al., 2018; Qin et al., 2020; Zhang et al., 2020b). The deep mud diapirs and gas chimneys in the Shenshu area are closely related to the gas hydrate accumulation (Chen et al., 2016; Su et al., 2016, 2017; Cheng et al., 2020), but how the diapirs/gas chimneys have shifted the BGHSZ, especially the influence of the associated diapiric faults on the gas migration and gas hydrate accumulation, remains unclear. The coexistence of gas hydrates and free gas has indeed been discussed by previous researchers based on logging data (Qian et al., 2018; Qin et al., 2020), but the mechanism of their coexistence has not been reasonably explained. Finally and most importantly, the transformation process and dynamic evolution after the formation of the gas hydrate system in the Shenhu area, especially the preservation conditions and controlling factors, which may determine the finial accumulation and distribution of the HGGHR, have not been fully disentangled. Based on high-resolution seismic data, drilling, logging, coring, sampling, and *in situ* testing, here we focused on the dynamic accumulation and preservation of the trial production of the HGGHR in the Shenhu area. The objectives and intentions of the research are (1) to characterize the HGGHR accumulated in the clayey silt-dominated sediments, (2) to investigate the deep structure controlling mechanism of the formation of the shallow HGGHR,

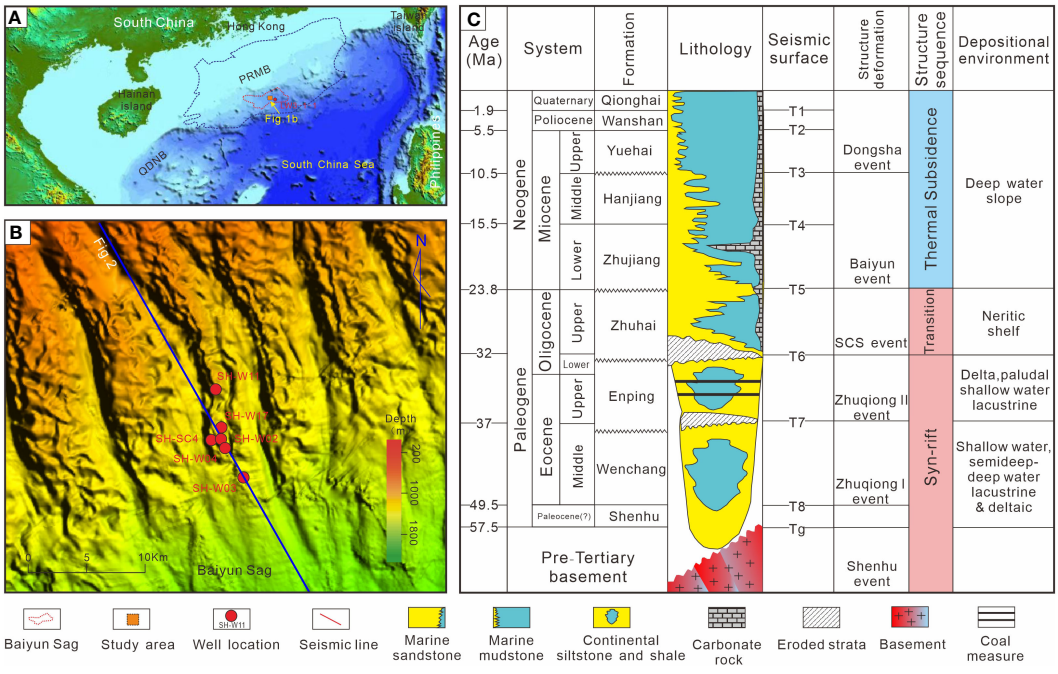

FIGURE 1
(A) Geographical location of the study area, which is structurely located in the Baiyun Sag of the Pearl River Mouth Basin (PRMB), northern South China Sea. **(B)** Submarine geomorphology and the location of boreholes drilled in the trail production gas hydarte reservoir in the Shenhu area. Comprehensive stratigraphic histogram of the Pearl River Mouth Basin (based on data from Pang et al., 2008). QDNB: Qiongdongnan Basin.

and (3) to reveal the dynamic evolution process and preservation condition of the HGGHR. Finally, a geological model of the dynamic formation of the HGGHR was developed, providing a geological reference for future HGGHR drilling, exploration, and development target optimization in submarine settings.

2 Geologic setting

The Shenhu gas hydrate trial production site is located in the middle of the northern continental slope of the northern SCS (Figure 1A). It has a water depth of 900–1400 m and is located 285 km from Hong Kong and 412 km from Guangzhou. The seabed topography of the trial production area is distinctly rugged, with multiple crisscrossing submarine canyons and ridges, which controls the distribution of the gas hydrates. Drilling and coring have revealed that the vast majority of the gas hydrates are concentrated in the shallow unconsolidated sediments associated with the submarine channel-levee systems (Figure 1B) (Zhang et al., 2020a).

The gas hydrate trial production site in the Shenhu area is structurally located in the Baiyun Sag in the southern deepwater area of the Pearl River Mouth Basin (PRMB). In the Cenozoic, it mainly underwent two tectonic evolution stages, Paleogene rifting and Neogene depression, and it experienced several regional tectonic events, forming a double-layer structure containing a lower rift and upper depression (Zhang et al., 2021) (Figure 1C). The lower structural units (Eocene-Lower Oligocene) were strongly faulted, and a series of grabens and half grabens formed. The upper structural units (Upper Oligocene-Quaternary) were dominated by regional thermal subsidence, the tectonic activity gradually weakened, and the depression was sequentially filled with terrigenous clastic sediments transported from the northern Paleo-Pearl River (Pang et al., 2008; Shao et al., 2008; Xie et al., 2013).

Since the Paleogene, lacustrian facies, marine-continental transitional facies, and bathyal-neritic facies strata have been deposited in the Baiyun Sag in succession, with a sedimentary thickness of up to 10 km. This provided the material basis for hydrocarbon generation. Drilling has proven that the Baiyu Sag is a large hydrocarbon-rich sag (Zhang et al., 2014). The lacustrine facies of the Eocene Wenchang Formation and the coal measure in the Oligocene Enping Formation are the main source rocks that have entered the mature to over-mature stage, generating a large amount of oil and gas and providing the hydrocarbon source of the conventional petroleum reservoirs, such as LW3–1, PY 30–1, and PY35–1. At present, the Miocene strata and its overlying strata, which contain abundant organic matter, are in the immature to low maturity stage and are entering the biogenic gas generation stage (Su et al., 2018, 2023). Gas hydrate drilling and coring have shown that both deep thermogenic gas and shallow biogenic gas could provide gas sources for the gas hydrate system (Zhang et al., 2019; Liang et al., 2022). Mud diapirs caused by the upward migration of deeply buried unconsolidated mudstone sediments under high pressure and gas chimneys resulting from intensive gas-bearing fluid activity are widely developed in the Baiyun Sag, providing efficient pathways for a large amount of thermogenic gas derived from a depth of thousands of meters and relatively shallow biogenic gas to be transported into the GHSZ (Chen et al., 2016; Su et al., 2016; Cheng et al., 2020). The gas hydrate reservoirs in the Shenhu area were mainly deposited within the Upper Miocene–Quaternary sediments, which are dominated by unconsolidated fine-grained clayey silt or silty clay and are generally characterized by a low cementation, high porosity, and low permeability (Wang et al., 2014; Su et al., 2016; Li et al., 2019). In addition, the gas hydrate reservoirs are rich in foraminifera fossils, which provide favorable reservoir space for pore-filling gas hydrates with a high saturation (Chen et al., 2011).

3 Data and methods

A 3-D seismic survey covering ~800 km^2 of the main Shenhu area was acquired by the Guangzhou Marine Geological Survey (GMGS) in 2018. The details of the seismic acquisition and processing of the raw seismic data have been introduced by Cheng et al. (2020). Based on the processed 3-D seismic data that were systematically interpreted using the Petrel software, in this study, from shallow to deep, the internal structure of the gas hydrate reservoir, and the distribution of the gas hydrates and free gas in the HGGHR were depicted in detail. In addition, the deep gas chimney and mud diapir and the associated diapiric faults under the HGGHR and the gliding faults in the GHSZ were also precisely identified and interpreted based on seismic variance analysis and the ant-tracking method.

The drilled boreholes used in this study included drilling and coring wells (SH-W11, SH-W17, and SH-W03) implemented to characterize the reservoir (Zhang et al., 2020b) before the implementation of the gas hydrate trial production and pilot drilling and logging wells (SH-W02 and SH-W04) constructed during the second trial production project (Qin et al., 2020). Logging while drilling (LWD) was implemented to obtain the natural gamma, calliper, acoustic time difference, neutron porosity, density porosity, nuclear magnetic resonance (NMR), and imaging logs, which provided a data basis for analyzing the occurrence of gas hydrates and free gas and for characterizing the lithology and physical properties of the reservoir (Qin et al., 2020; Ye et al., 2020). The Herron Equation was used to calculate the reservoir permeability (Herron, 1987). The saturations of the gas hydrates and associated free gas were calculated based on the NMR and density logs, and the details of the method have been described by Collett (2013) and Akihisa et al. (2002). In addition, the nuclear magnetic permeabilities were calculated using the Timur formula (Timur, 1969), so the nuclear magnetic permeability of the gas hydrate layer was taken as the initial permeability when the gas hydrates were not decomposed. In the gas layer, the input of the nuclear magnetic permeability (free fluid porosity and total porosity) was affected by the gas, resulting in a lower nuclear magnetic permeability than the actual permeability.

Based on microscopic interpretation of the high definition (HD) resistivity imaging data and seismic interpretation and attribute analysis, we identified and characterized the possible faults in the

GHSZ to explore the relationship between the faults and the distribution of the gas hydrate-bearing layers and free gas-bearing layers. A well-tie profile was constructed to show the vertical and lateral variations in the gas hydrate-bearing sediments. In addition, inversion of the acoustic impedance and velocity was conducted using the Jason software, and the inversion results provided a direct basis for the identification and analysis of the potential gas hydrates and free gas within the HGGHR.

Geochemical analysis of the hydrate-bound gas collected from well SH-W04 was conducted offshore using an INFICON MicroGC Fusion gas chromatograph with a molecular sieve, PLOT Q column, and thermal conductivity detector (Wei et al., 2018). The gas compositions were quantitatively analyzed to determine all of the C1–C5 components. The details of the experimental method have been described by Zhang et al. (2019). Due to the equipment limitations on board, the hydrogen and carbon isotopes of these gases were not analyzed. Based on the gas compositions and geothermal detection data acquired from well SH-W04, the gas hydrate phase equilibriums with different gas compositions were modeled by using the CSMHYD software (Sloan, 1998). In addition, the bases of the GHSZs were calculated by crossing the different phase equilibrium curves and the geothermal gradient confirmed via *in situ* testing and they were compared with the BSR interpreted from the seismic profile to discuss the possible different structures of the gas hydrates (structure I, SI and structure II, SII).

4 Results

4.1 Seismic interpretation

The trial production of the HGGHR was conducted on the pitching end of a submarine ridge (Figure 1B). The high-resolution 3-D seismic profile shows that a large mud diapir is developed beneath the gas hydrate reservoir. The root of the diapir originates in the Wenchang Formation (below T7). The mud diapir has a width of >4 km and a vertical depth of ~2.7 km, and the diameter of the main body is ~3 km. Acoustic chaotic reflections were observed in the interior of the mud diapir, and pulled–up events caused by the upward arch traction of the mud source material were also distinctly observed on both flanks of the mud diapir. In the vicinity of the deep section of the mud diapir (T6), a high amplitude reflection (bright spot) with a continuous length of more than 4 km was identified (Figure 2A). Faults of different scales were observed on the top and flanks of the mud diapir. The fault assemblage formed a positive flower-like structure and extended upward into the GHSZ. Bright spots were observed above the top of the flower-like fault system. In addition, acoustic blanking with internal pulled-down features occurred in the upper sections of the mud diapir (Figures 2–4). By extracting the variance attribute, the shape and location of the fault were accurately identified (Figure 3A). In the instantaneous frequency attribute profile, low instantaneous frequency stratigraphic reflections were observed in the interior of the mud diapir and the diapir-associated fault development area, and the signal was obviously lower than that of the surrounding rocks (Figure 3B).

Double bottom simulating reflectors (double BSRs) were identified in the HGGHR (Figure 4). The upper BSR1 (~230 mbsf at site SH-W04, meters below the seafloor) with a transverse extension of ~3 km exhibits an anticline feature that is roughly parallel to the seafloor and clearly crosscuts the ambient strata, with a negative reflection polarity compared to that of the seafloor. Above BSR1, there is a patch with a high amplitude reflection, which is thick on the left side and relatively thin on the right side (Figure 4A). Drilling confirmed that these high amplitude reflections are gas hydrate bearing sediments (Li et al., 2018). The region underlying BSR2 (~320 mbsf), with an extension of approximately 1-km and 90-m intervals from BSR1, also mimics the seafloor with a negative reflection polarity. In addition, distinct inclined high amplitude reflections were observed between the double BSRs and beneath BSR2.

Based on the high-resolution 3-D seismic data, a series of faults were identified in the HGGHR in vertical and plane views (Figures 2–5). These faults can be divided into three groups. The first group (FIa, FIb, FIc, FId, FIe, and FIf) contains the diapir-associated faults that cut through the T5 interface but do not cut the GHSZ (Figures 2, 3). The second group contains the overlying diapir-associated faults (FIIa, FIIb, FIIc, FIId, and FIIe) derived from the strata over the T5 interface and extend through the GHSZ (Figure 4). The third group (FIIIa, FIIIb, FIIIc, FIIId, and FIIIe) contains the NE-striking gliding faults identified in the gas hydrate reservoir. Several FIII faults extend nearly to the seabed, controlling the boundary of the gas hydrate reservoir's distribution. Fault FIIIa cuts the gas hydrate bearing layer and BSR2 and continues to extend downward. Fault FIIIb cuts BSR1 and extends downward, and fault FIIIc terminates at BSR1. Faults FIIId and FIIIe control the outer boundary of the gas hydrate reservoir. The fault displacements are small, but there is some difference in the thickness of the gas hydrate bearing layer and free gas, which is indicated by the high amplitude on both sides of the fault. In general, the thicknesses of the gas hydrate-bearing and gas-bearing layers are larger in the footwall (~80–~20 m) of the fault than in the hanging wall (0–~30 m) of the fault (Figure 4).

4.2 Inversion results

The inversions of the acoustic impedance and velocity also clearly revealed the internal structural characteristics of the HGGHR (Figure 6). Generally, the strata above BSR1 exhibited a high impedance contrast and high stratigraphic velocity, while the strata between the double BSRs and beneath BSR2 exhibited a relatively lower impedance contrast and relatively lower stratigraphic velocity. In addition, the gas hydrate-bearing layer, free gas-bearing layer, and double BSRs could be inferred from the inversion profiles, and their vertical and lateral extensions were also identified, providing information for accurately interpreting the gas hydrates and free gas, with the seismic and LWD interpretation taken into account.

The reflection amplitude of BSR1 in the HGGHR was too strong, posing a certain shielding effect on the reflection of the underlying strata. An accurate well-to-seismic calibration could not be conducted, which inevitably led to some errors in the inversion

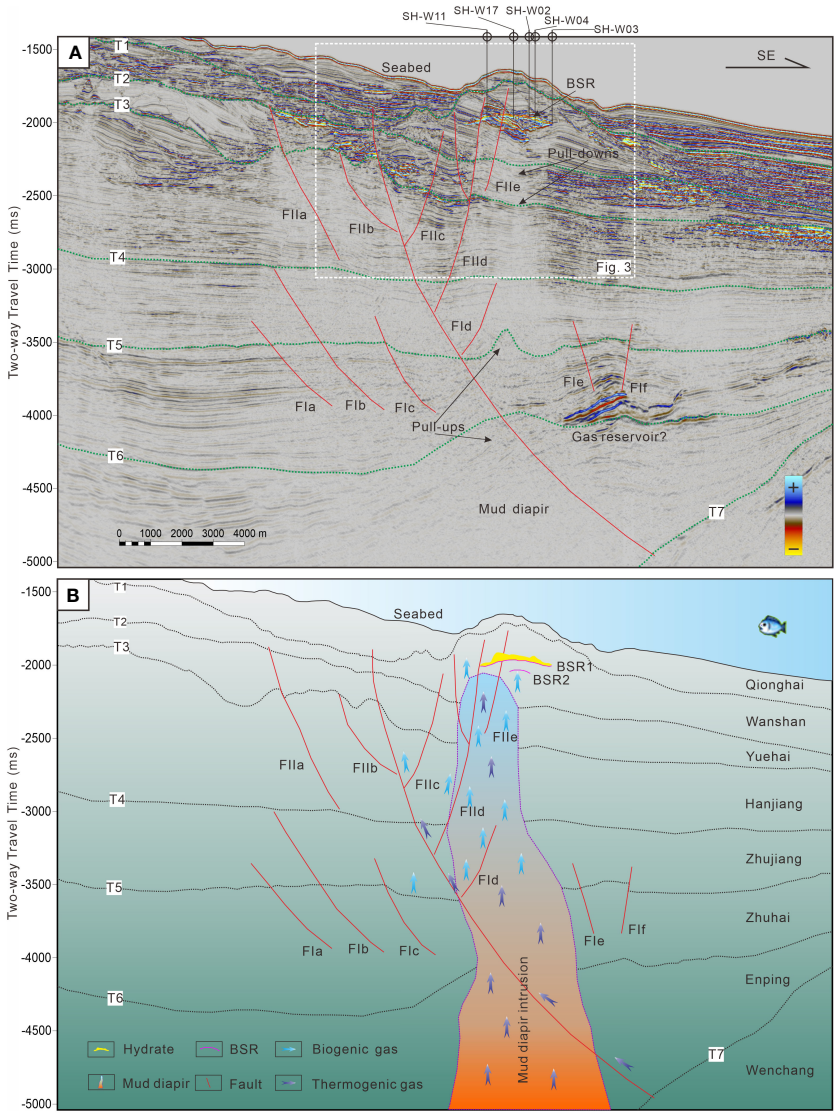

FIGURE 2
(A) Seismic reflection profile and **(B)** geological interpretation of the trial production gas hydrate reservoir in the Shenhu area. The location of the seismic profile is shown in Figure 1B.

and logging results. In addition, the gas hydrates beneath BSR1 coexisted with the gas-bearing layer, which weakened and attenuation of the seismic wave signal, and the seismic wave did not effectively preserve the information about the gas hydrates below BSR1. Therefore, the inversion results cannot show the high wave velocity formation indicating gas hydrates beneath BSR1, and the overall reflection is characterized by a low wave velocity. However, this inversion result cannot be used to rule out the occurrence of gas hydrates beneath BSR1.

4.3 Logging responses

Multiple exploration wells and parameter boreholes were drilled in different locations of the HGGHR to further reveal the distribution characteristics of the gas hydrates and associated free gas (Figures 2, 4, and 7).

Generally, the gas hydrate-bearing layer shows low gamma values, which are related to the abundance of foraminifera in the reservoir sediments. Because the reservoir is filled with gas hydrates, both the density log and the neutron porosity values are lower than hydrate-free layers. The Formation MicroScanner image (FMI) logging curve corresponding to the abnormal high resistivity and low acoustic time difference contains distinct bright features, indicating the occurrence of gas hydrates. It can be seen from the well tie profile that the thickness of the interval with logging anomalies above BSR1 gradually thins from NW to SE (Figure 7). From well SH-W17 to well SH-W02, the thickness of the interval containing the gas hydrate-bearing layers decreases from ~68 m to 0 m. From well SH-W02 to well SH-W03 located in the right

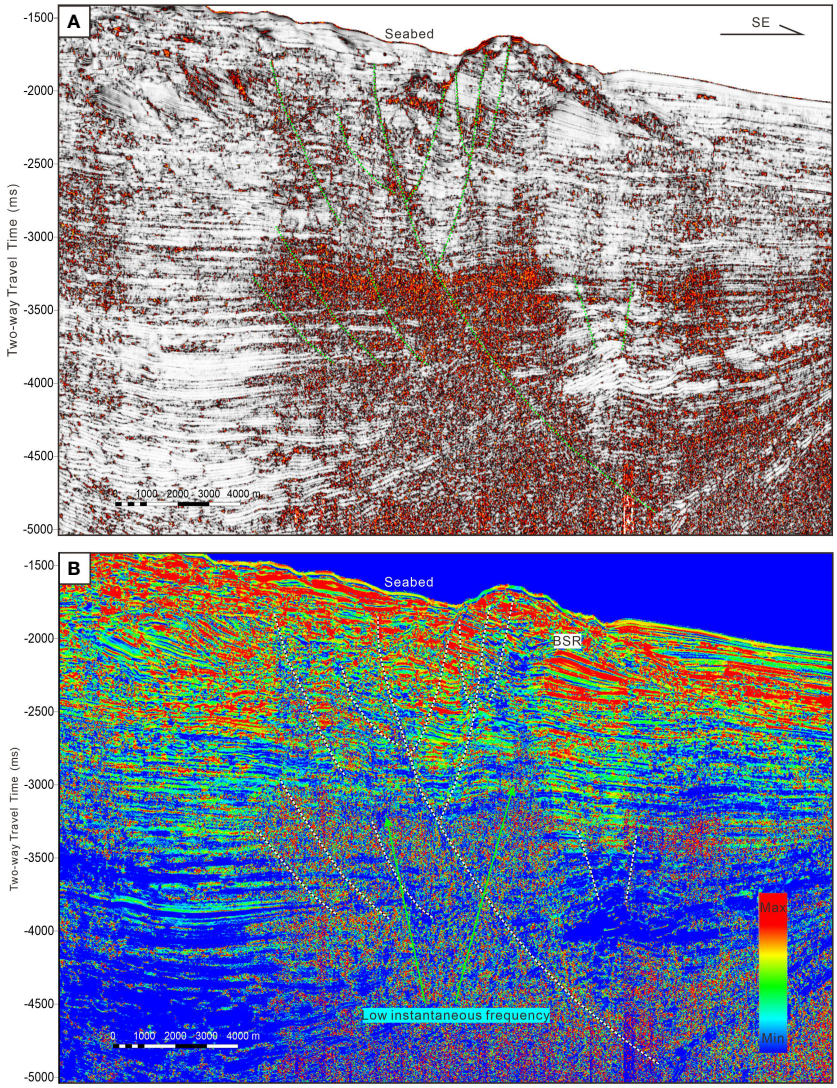

FIGURE 3
(A) Variance attribute shows the deep fault structure in the gas hydrate accumulation; **(B)** Instantaneous frequency profile shows possible hydrocarbon migration in the trail production gas hydrate reservoir.

termination of BSR1, the logging results show that the logging curve is almost flat and there is no gas hydrate response (Figure 7), indicating that the right terminus of BSR1 is the right boundary of the gas hydrate reservoir. To characterize the structural features of the strata within the GHSZ, geoVISION logs were analyzed. The geoVISION profile of well SH-W11 shows that minor SE and NNE trending faults (blue T-shaped tadpole) are developed at ~1442 m and 1474 m, respectively (Figure 8A). A minor NW-trending fault is developed at ~1543.5 m in well SH-W17, with a broad fault surface, and corrosion marks can be seen on the surface. In addition, deformed beddings were observed overlying this minor fault (Figure 8B). A minor NNW-trending fault was identified at 1467.6 m in well SH-W02. This microfault has a small width and high resistivity at the fault interface. The occurrence of the deformed bedding above and below the fault is different, and the deformed beddings above the fault mainly trends NW, while the deformed beddings below the fault trends SW (Figure 8C). No minor fault was observed in well SH-W03; however, deformed beddings were commonly identified on the geoVISION profile (Figure 8D).

4.4 Accumulation characteristics of gas hydrate reservoir

The drilling and coring results show that the distribution characteristics of the gas hydrates in the reservoir are in good agreement with the results of the seismic interpretation and LWD analysis. The gas hydrate-bearing layer is mainly located within the section with high amplitude reflections above BSR1, and it corresponds to the high resistivity, low acoustic time difference, and high brightness layer in the imaging logging on the LWD profile. The top of the gas hydrate-bearing layer is mainly located at 207.5–230 mbsf; and the base of the gas hydrate-bearing strata identified by logging is located at 230–270 mbsf. The thickness of the gas hydrate-bearing zone is 0–62.5 m. It

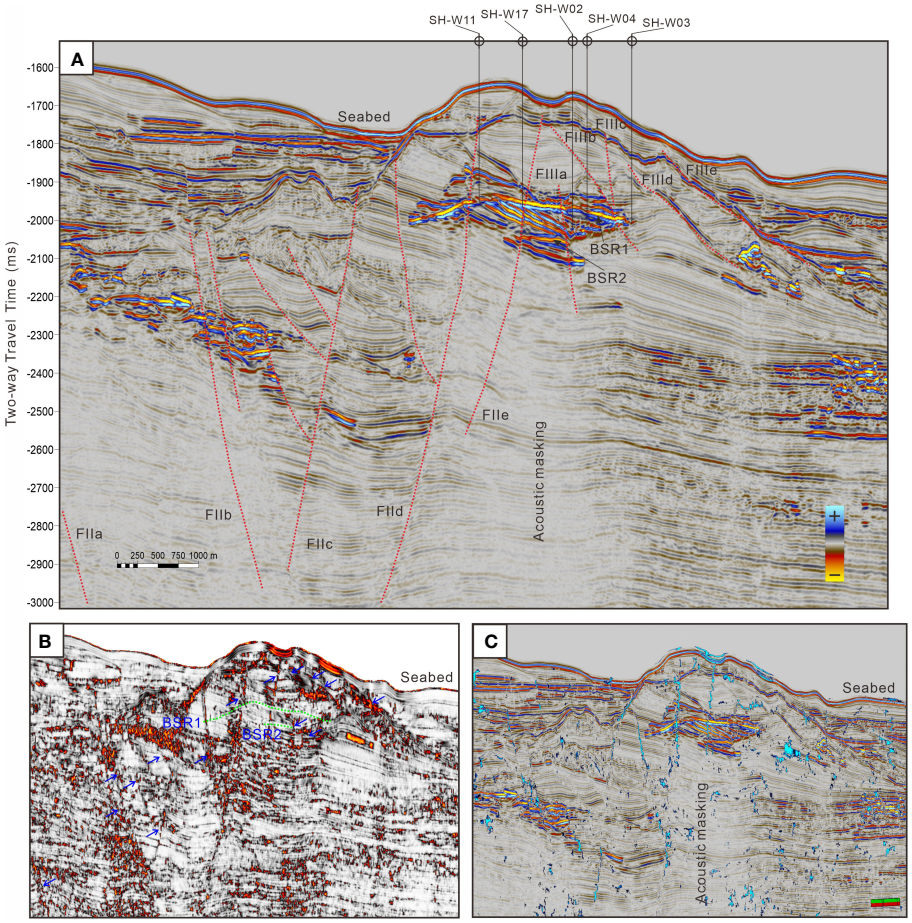

FIGURE 4
(A) Enlarged image shows the detailed features of the gas hydarte accumulaton and fault development in the trial production gas hydrate reservoir in the Shenhu area. **(B)** Variance attribute shows the possible faults in the gas hydrate accumulation. **(C)** Ant tracking profile shows the potential faults and cracks in the gas hydrate accumulation.

can also be observed from the well tie profile (Figure 7) that there are still abnormal resistivity and acoustic time difference areas beneath BSR1, indicating that gas hydrates still exist beneath BSR1. The drilling results for well SH-W17 confirm the occurrence of SII gas hydrates below BSR1 (Zhang et al., 2020b). In addition, the drilling results for well SH-SC4 from the first gas hydrate trial production in the Shenhu area also confirm the coexistence of gas hydrates and free gas beneath BSR1 (Li et al., 2018).

The logging curves (Figure 9) for well SH-W02 (water depth: 1240 m), which is located in the central part of the gas hydrate

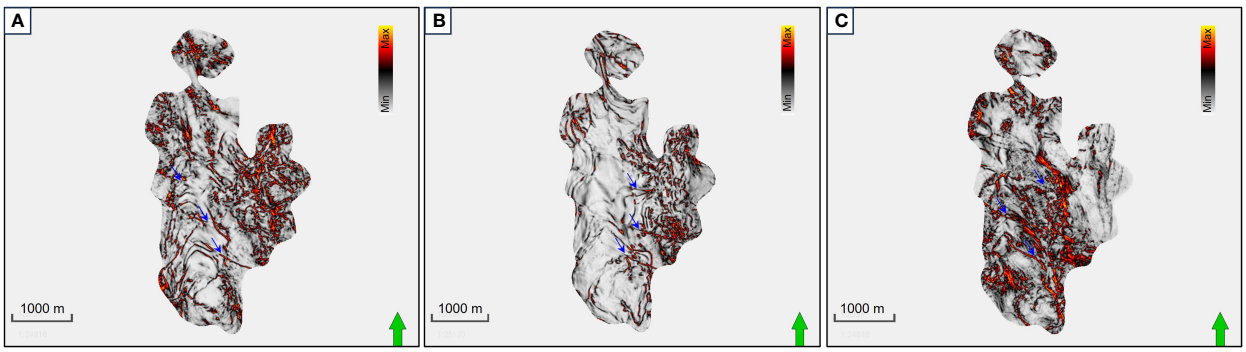

FIGURE 5
Plane view of variance attribute showing the distribution of faults in the high-grade gas hydrate reservoir (HGGHR). **(A)** Variance attribute of -100 ms below BSR1; **(B)** Variance attribute of BSR1; **(C)** Variance attribute of +100 ms above BSR1.

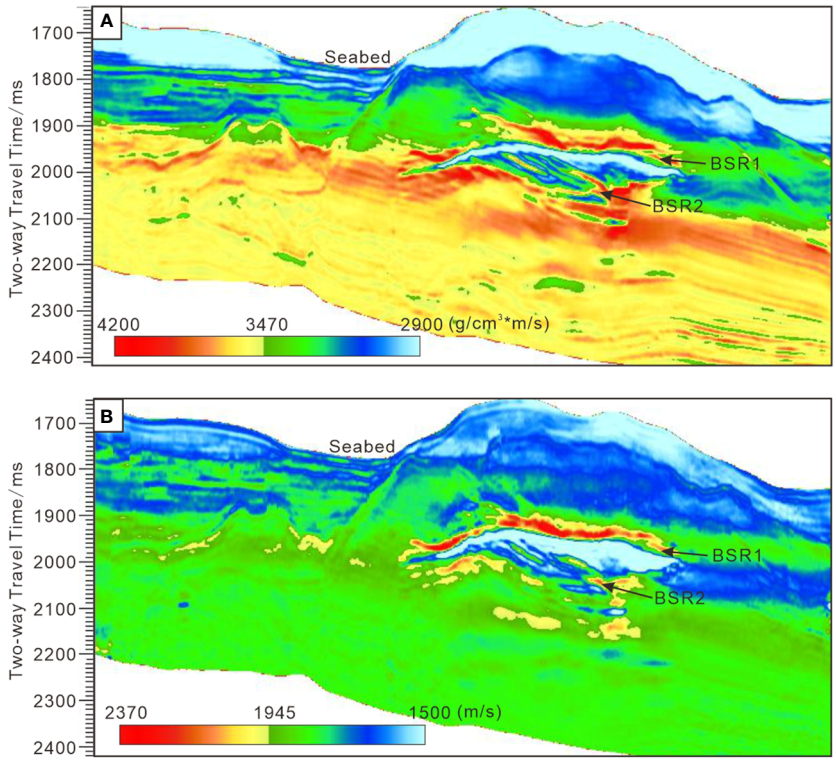

FIGURE 6
Characteristics of **(A)** impedance inversion and **(B)** velocity inversion of the trail production gas hydrate reservoir in the Shenhu area.

reservoir, show that in the 1450–1498 m interval, the resistivity increases, the p-wave time difference decreases, and the neutron density does not change significantly, indicating the presence of a gas hydrate-bearing layer. According to the log interpretation and calculation results, the thickness of the gas hydrate-bearing layer is 48 m, the average effective porosity is 37.3%, the average gas hydrate saturation is 31.5%, and the average permeability is 0.24 mD. In the 1498–1545.5 m interval, the resistivity and the p-wave time

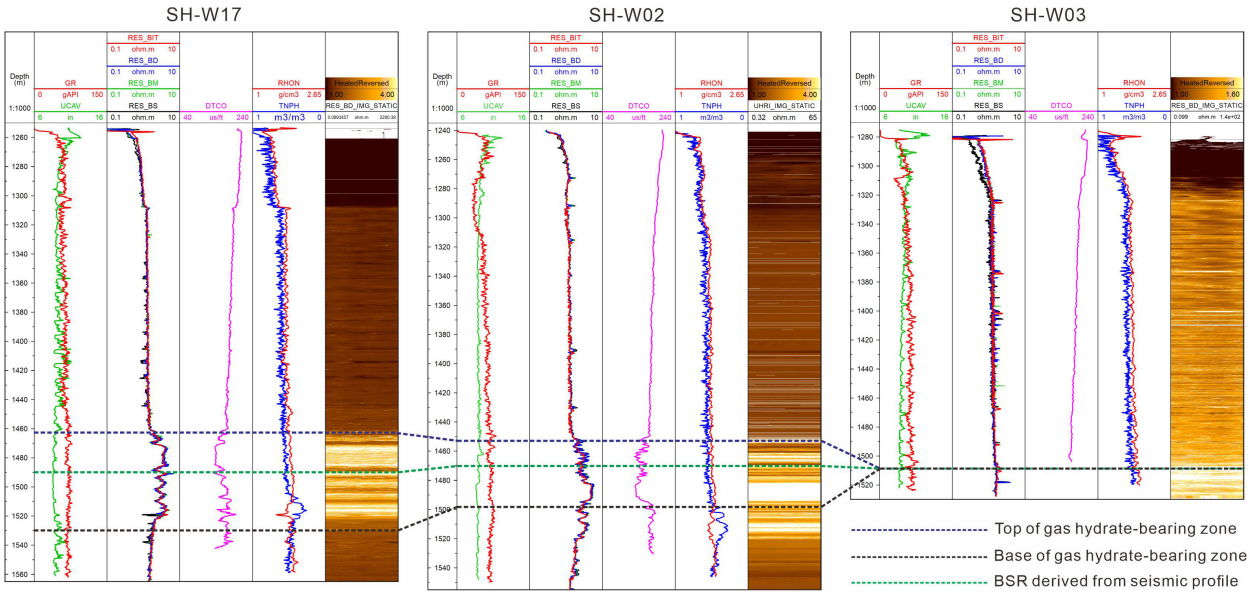

FIGURE 7
Well-tie shows the logging response characteristics and comprehensive interpretation of gas hydarte and free gas in the trail production gas hydrate reservoir in the Shenhu area.

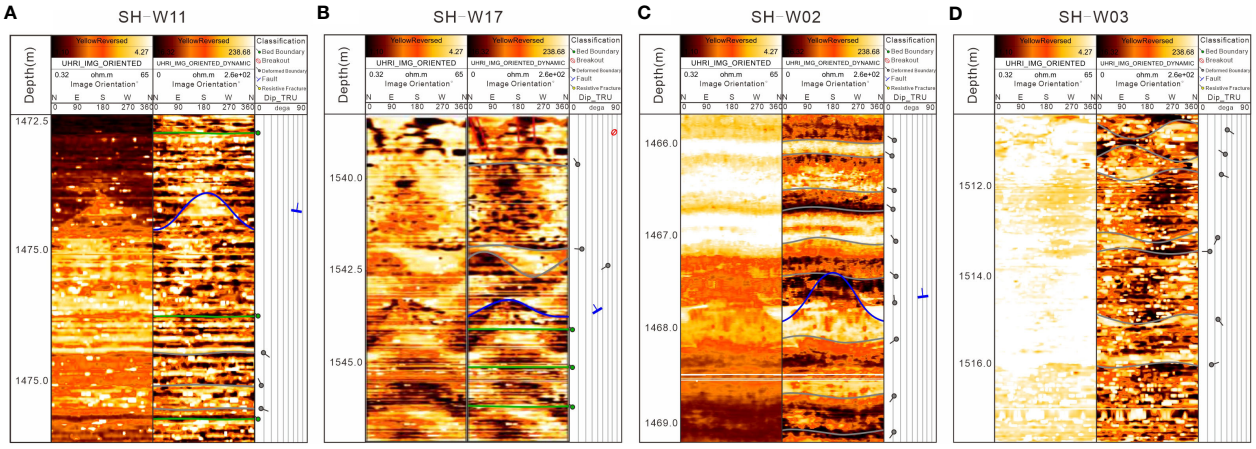

FIGURE 8
(A) Minor SE and NNE trending faults are identified at ~1442 m and 1474 m in well SH-W11; **(B)** NW-trending fault and deformed beddings are observed overlying this minor fault in well SH-W17; **(C)** Minor NNW-trending fault and deformed beddings are identified in well SH-W02; **(D)** Deformed beddings are commonly observed in well SH-W03.

difference increase, and the neutron and density log cross backward, which is the response of the gas-bearing layer. However, in this interval, the imaging log still contains a bright layer, and the resistivity log exhibits fluctuations with elevated values. According to the log interpretation results for adjacent well SH-SC4 (Li et al., 2018), this interval is interpreted as mixed layers in which gas and gas hydrates coexist. Based on the gas saturation, the gas-bearing layer was divided into a high saturation gas-bearing layer and a low

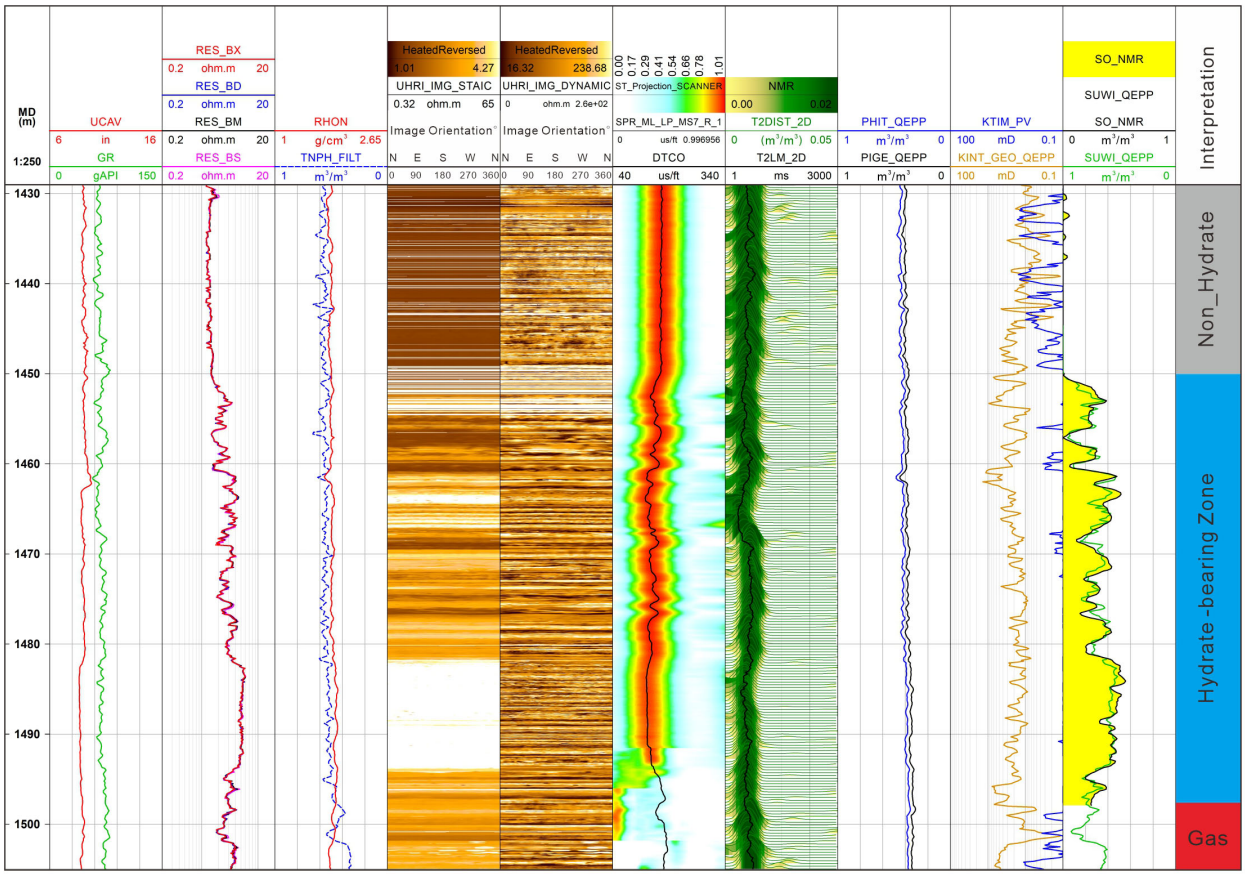

FIGURE 9
Logging while drilling profile of well SH-W02 shows the features of gas hydrate-bearing zone.

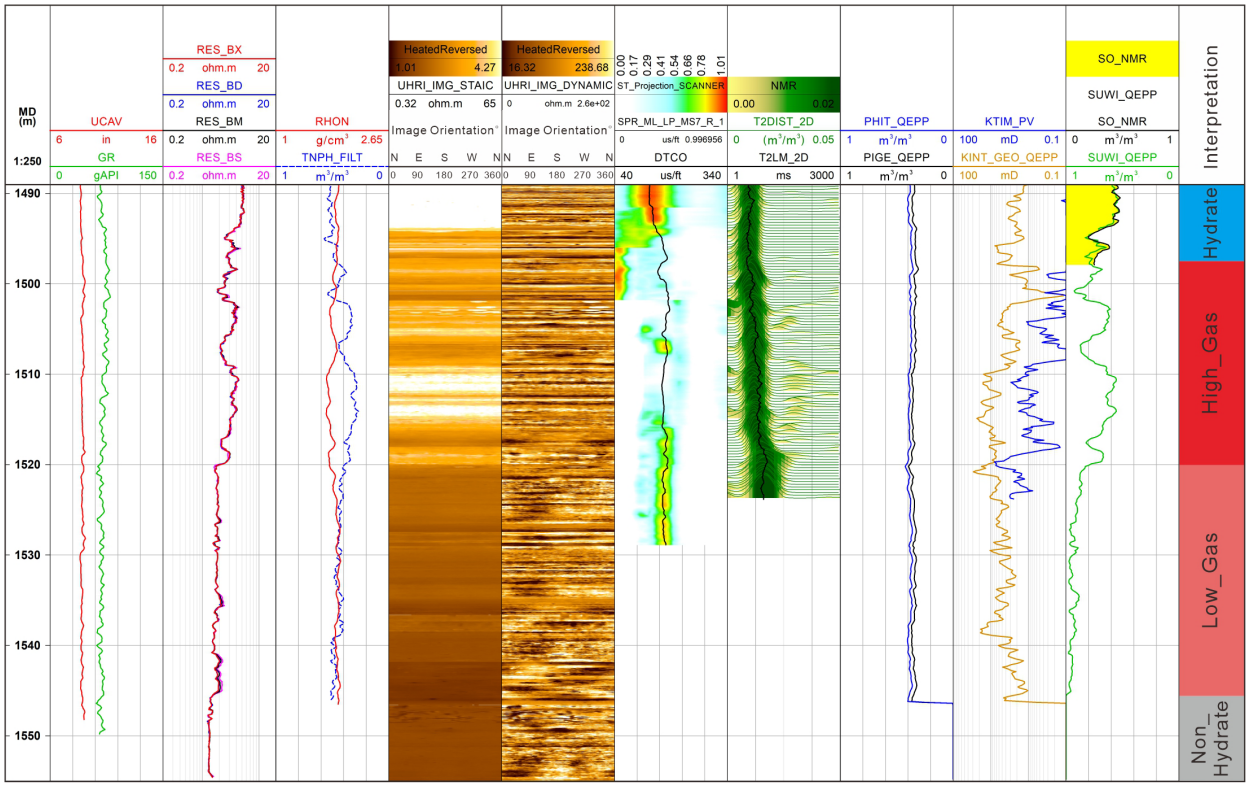

FIGURE 10
Logging while drilling profile of well SH-W02 shows the features of free gas-bearing zone below the gas hydrate-bearing zone.

saturation gas-bearing layer (Figure 10). The high-saturation gas-bearing layer is located at 1498–1520 m and is 22 m thick. It has an average effective porosity of 34.6%, an average gas saturation of 32.1%, and an average permeability of 1.26 mD. The low saturation gas-bearing layer is located at 1520–1545.5 m and is 25.5 m thick. It has an average effective porosity of 34.4%, an average gas saturation of 7.0%, and an average permeability of 1.08 mD. Overall, the distribution characteristics of the gas hydrates and associated free gas and the reservoir's porosity and permeability revealed by several wells drilled in the gas hydrate reservoir are basically similar (Table 1), and the gas hydrate reservoir is characterized by a high porosity and low permeability.

4.5 Characteristics of gas hydrate core sediments

Pressure coring in the gas hydrate reservoir confirmed that the lithology is characterized by interbedded grey-green clay, grey-green silty clay, and grey-green clayey silt (Figure 11A), and the silt content

TABLE 1 Distribution and physical properties of hydrate-bearing layer and free gas-bearing layer in the trial production gas hydrate reservoir in the Shenhu area.

Borehole	Depth (mbsl)	Reservoir type	Porosity (%)	Permeability (mD)	Mean hydrate saturation (%)	Reference
SH-W17	1460-1510	Hydrate	33.2	0.2	33	Zhang et al., 2020b
	1510-1522	Hydrate + Free gas	34	2.1		
SH-W02	1450-1498	Hydrate	37.3%	0.24	31.5	
	1498-1545.5	Hydrate + Free gas	34.4-34.6	1.08-1.26		
SH-SC4	1495-1530	Hydrate	35	2.9	34	Li et al., 2018
	1530-1545	Hydrate + Free gas	33	1.5	31	
	1545-1572	Free gas	32	7.4		

10.3389/fmars.2024.1418716

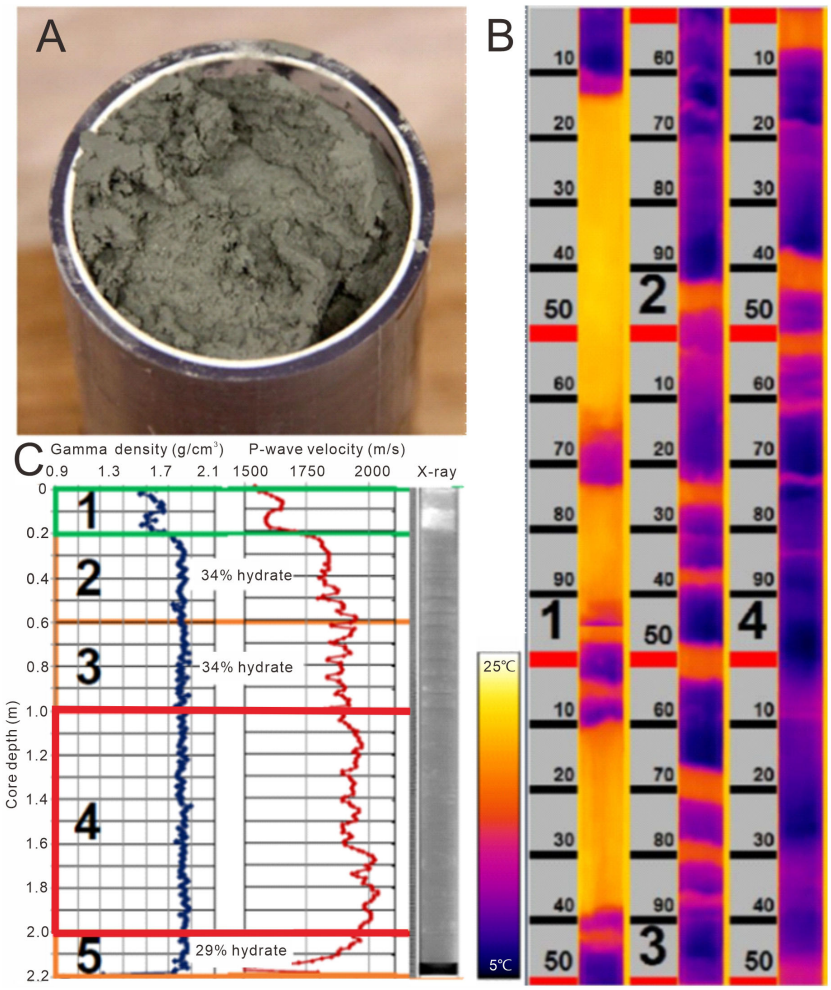

FIGURE 11
Characteristics of pore-filling gas hydrate core recovered from well SH-W04 in the trial production gas hydrate reservoir. **(A)** Grey-green silty clay core sediment, 209 mbsf. **(B)** Infrared scan of the gas hydrate-bearing layer of pressure core shows low temperature anomalies. **(C)** X-ray scanning and P-wave velocity analysis of gas hydrate core, 207.5 mbsf.

increases with depth. In addition, the infrared scan of the core shows that the sediments exhibit significant low temperature anomalies, indicating the presence of gas hydrates (Figure 11B). In the case of well SH-W04 (water depth of 1270 m), foraminifera were found in the shallow core sediment at 225 mbsf, and all of the cores had a strong oil smell. At 230 mbsf, the core was dense and the water content was low. The X-ray scan of the core shows that the gas hydrate-bearing layer is a dark layer, and there is no indication of fracture-filling gas hydrates, which are characterized by bright layers or blocks. The gamma density of the corresponding layer is relatively low, while the velocity analysis shows that the P-wave velocity ranges from 1750 m/s to ~2000 m/s, which is higher than that of the non-hydrate bearing layer. In addition, no gas hydrates visible to the naked eye were observed in the recovered pressured cores, so it is plausible to conclude that the high-speed section shown by the P-wave velocity of the pressure core corresponds to the interval containing pore-filling gas hydrates (Figure 11C). This is similar to boreholes SH-W11 and SH-W17, which were previously drilled in the trial production gas hydrate reservoir (Zhang et al., 2020b).

4.6 Gas hydrate saturation

According to the quantitative degassing mass balance calculation of the gas hydrates from the pressure core, the gas hydrate saturation (proportion of pore space volume) above the base of the methane gas hydrate stability zone ($BGHSC_1$) in well SH-W04 is 21–41% (Figure 12A), and the average gas hydrate saturation calculated from the pressure core (207.5 mbsf) degassing is 29–34% (Figure 12A). Below $BGHSC_1$, the free gas saturation (proportion of pore space volume) reaches 30%. Because the gas hydrates in the pressure cores are mainly stored in liquid nitrogen or a pressured tank for subsequent analysis, they cannot completely reflect the preservation state of the gas hydrates under *in situ* temperature and pressure conditions, and the actual gas hydrate saturation should be greater than the measured value. The geochemical analysis of the pore water showed that the chloride in the vicinity of $BGHSC_1$ exhibited a distinct desalination anomaly (chloride baseline = 520 mM), indicating the occurrence of gas hydrates. The maximum gas hydrate saturation calculated via the

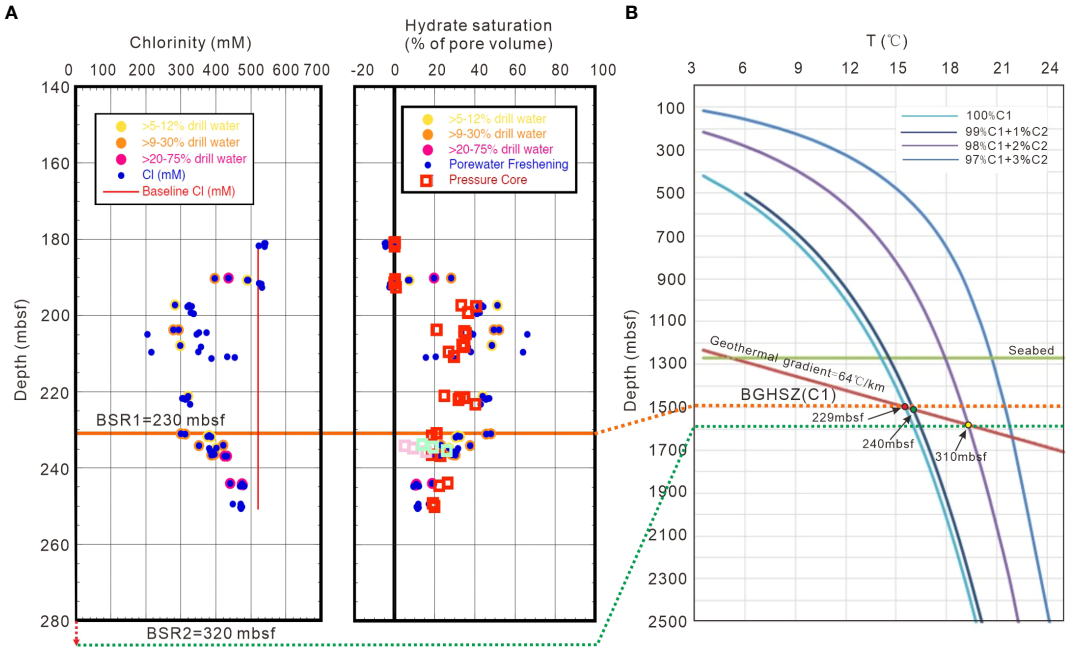

FIGURE 12
(A) Gas hydrate saturation variation with depth in well SH-W04. All points, regardless of depth, are calculated as gas hydrate, both from porewater freshening analysis and pressure core quantitative degassing methane mass balance. Green and pink points are alternate sets of methane concentrations for pressure Core SH-W04–21A; **(B)** Hydrate phase equilibrium simulation curve under different gas components in well SH-W04 (estimated geothermal gradient of 46°C/km and pore water salinity of 3.5% by temperature and pressure dispersal test). BGHSC1: Base of gas hydrate stability zone of 100% CH_4.

TABLE 2 Component characteristics of gas released from pressure retaining core of well SH-W04 of hydrate reservoir in the Shenhu area.

Depth mbsf	C1%	C2 ppm	C3 ppm	iC4 ppm	C4 ppm	C5 ppm	iC5 ppm	C1/C2
181.4	98.4	2932	10572	974	756	354	b.d.	336
190.40	99.4	1966	1791	192	827	796	b.d.	506
197.16	99.4	5340	689	49	49	13	b.d.	186
198.96	99.1	6487	2037	150	84	trace	154	153
204.65	99.4	5676	171	trace	14	trace	b.d.	175
208.10	99.3	4891	2128	136	99	13	b.d.	203
210.40	99.4	4749	609	40	50	31	171	209
221.63	99.3	4471	1823	153	54	14	124	222
223.19	99.0	4658	4913	425	149	35	148	212
231.30	99.4	4370	782	80	87	53	175	228
233.74	99.5	3661	893	108	65	27	b.d.	272
235.00	99.4	3894	1065	135	80	30	418	255
236.80	99.5	3922	1040	127	67	22	215	254
244.50	99.5	3937	1026	124	71	25	164	253
249.80	99.4	3898	1065	142	89	42	267	255
259.90	99.5	4575	460	43	50	29	116	217
264.24	99.4	4546	672	81	88	54	166	219

mbsf, meters below the seafloor; trace, below 30ppm; b.d., below detection limit (10 ppm).

porewater freshening was >60%. In addition, the gas hydrate saturation calculated using the pressure core quantitative degassing mass balance is in good agreement with the variation trend of the gas hydrate saturation with depth calculated via the pore water freshening, and the gas hydrate saturation is generally 20–50% (Figure 12A).

4.7 Geochemical characteristics of hydrate-bound gas

Logging, pressure coring and conventional (non-pressure) coring operations, as well as core fluid and gas geochemical analysis (Table 2), were performed for well SH-W04 in the HGGHR. The test results show that methane was the predominant component of the hydrocarbons collected from the cores. Most of the gas samples contained more than 99% methane, and the ethane contents were 1966–8430 ppm. In addition, the propane content was >1% concentration, and small amounts of butane, isobutane, pentane, and isopentane were also detected. The C1/C2 ratios of all of the gas samples were less than 1000. Due to the limitations of the testing equipment, the isotopes of the methane and C_2+ hydrocarbons from this well were not analyzed.

5 Discussion

5.1 Factors controlling formation and accumulation of the HGGHR

5.1.1 Mud diapir controls hydrocarbon migration and shifts the GHSZ

The high-resolution seismic profile shows that a large mud diapir derived from the Wenchang Formation and diapir-associated faults of different scales are developed beneath the BGHSZ of the HGGHR (Figure 2). Generally, these vertical structures are favorable pathways for hydrocarbon migration and can promote the transportation of deep thermogenic gas and shallow biogenic gas into the GHSZ (Figures 3, 4), as has been discovered in many other mud diapir development areas (Lüdmann and Wong, 2003; Ning et al., 2009; Hsu et al., 2017). This indicates that the occurrence of thermogenic gas in the hydrate-bound gas recovered from the HGGHR is the result of vertical transportation via the mud diapir. In addition, faults with different patterns, especially the flower structure fault assemblage extending upward into the GHSZ, are developed in the vicinity of the mud diapir, facilitating the migration of deep hydrocarbons (Figures 2–4). Moreover, the development and evolution of the mud diapir may have affected the P-T conditions of the GHSZ, as the activity of mud diapirs can lead to localized thermal anomalies (Chow et al., 2000). Elevated temperatures induced by the mud diapir may inhibit gas hydrate precipitation, alter the BGHSZ, and even lead to the dissociation of gas hydrate and gas seepage (Lüdmann and Wong, 2003; Feseker et al., 2009; Crutchley et al., 2014; Smith et al., 2014). In the early to middle stage of the formation of the mud diapir, the accompanying thermal fluid activity was limited, and the associated structures such as the diapiric-associated faults in the top of the diapir were not well developed, so they may have had little influence on the GHSZ. In the late stage of diapir development, the scale of the diapir and the associated faults developed further, the thermal fluid activity was enhanced, and the P-T conditions in the shallow strata were altered, resulting in variation of the GHSZ and possible gas hydrate dissociation. This process has been demonstrated in nearby drilling site SH5 where a mud diapir with geothermal anomaly has resulted in complete dissociation of gas hydrate (Wan et al., 2017). We propose that due to the increase in the temperature of the strata caused by the ascending thermal fluids, some of the gas hydrates decomposed and free gas was released. Part of the BSR remained to form the paleo BSR2, and the BGHSZ was shifted upward accordingly. BSR2 observed in the seismic profile may be the paleo BSR formed under the P-T conditions before the diapir affected the GHSZ. As the mud diapir is inactive at present (Cheng et al., 2020), the current thermal state of the gas hydrate system is in equilibrium, which is suitable for hydrate formation and accumulation. As a consequence, some of the released free gas and the additional gas that has migrated upward through the mud diapir reprecipitated as gas hydrates, causing the appearance of the present BSR1 in the seismic profile. Finally, double BSRs and the coexistence of gas hydrates and free gas were identified in the HGGHR. Other factors, such as sea level rise and seabed temperature variation caused by global warming since the Last Glacial Maximun may also have resulted in the shift of the BGHSZ and the dynamic hydrate system, but present data is beyond the scope of our discussion.

5.1.2 Sufficient dual supply of biogenic gas and thermogenic gas

Geochemical analysis of the gas hydrates obtained during the GMGS3 and GMGS4 drilling expeditions in the gas hydrate trial production zone in the Shenhu area revealed that (Zhang et al., 2019) the main gas composition of the hydrate-bound gas is CH_4 (>99%). In addition, heavier hydrocarbons (C_3+) were detected in the pressure core and non-pressure core hydrate-bound gas, the maximum propane concentration is greater than 1%, and trace amounts of butane, isobutane, and pentane were also detected in the hydrate gas samples. Geochemical testing of production hydrate gas recovered from the first trial production reservoir in 2017 revealed that the gas composition is overwhelmingly dominated by methane (Ye et al., 2018). However, the carbon and hydrogen isotope analysis results for the hydrocarbons obtained during expeditions GMGS3 and GMGS4 and the two trial production tests revealed that (Ye et al., 2019; Zhang et al., 2019; Liang et al., 2022) the hydrate-bound gas is a mixture of biogenic gas and thermogenic gas, with a bias towards biogenic gas. The above geochemical analysis of the hydrate-bound gas obtained through coring in well SH-W04 in the HGGHR in 2019 also provided evidence of biogenic gas and thermogenic gas supplies for the formation of gas hydrates with a high saturation (Ye et al., 2019). Based on comparison of the isotopic compositions of the methane and other hydrocarbons in the hydrate-bound gas and natural gas obtained from conventional reservoirs in the Baiyun Sag, it was found that the shallow gas hydrate reservoir and deep conventional reservoirs are superimposed, and they have a homologous symbiotic relationship (Zhang et al., 2019; Liang et al., 2022). In addition,

the trial production of the HGGHR was conducted close to gas field LW3–1 in the Baiyun Sag (Figure 1A), so the hydrocarbon supply should be sufficient, as demonstrated by the above deep mud diapir induced gas chimney and the bright spot on the seismic profile (Figures 2–4). According to the hydrocarbon generation and expulsion history of the Baiyun Sag, the geological background of the gas hydrate accumulation, and the characteristics of the hydrate-bound gas in the Shenhu gas hydrate trial production area (Wang et al., 2014; Zhang et al., 2014; Su et al., 2018; Zhang et al., 2019), it was found that sufficient supplies of biogenic gas and thermogenic gas provided the basis for the formation and accumulation of the HGGHR in the Shenhu area.

5.1.3 Recycling of free gas and dynamic formation of gas hydrates

Based on the above results of the seismic interpretation, acoustic impedance and velocity inversion, logging, and coring tests, the coexistence of gas hydrates and free gas was confirmed in the HGGHR in the study area, which has been reported by previous researchers (Qian et al., 2018; Qin et al., 2020). The pressure coring confirmed that high saturation gas hydrates are distributed above BSR1 in well SH-W04. Beneath BSR1 (BGHSC1), chloride freshening has been identified (Figure 12A). Therefore, it is plausible to speculate the presence of *in situ* SII gas hydrates beneath BSR1 in well SH-W04, similar to other provinces confirmed by coring and/or logging (Paganoni et al., 2016; Liang et al., 2017). The strata above BSR1 in well SH-W02 contains *in situ* gas hydrates, and all of the core samples from below BSR1 contain *in situ* free gas. In adjacent well SH-SC3, SII gas hydrates were also detected beneath BSR1 via laser Raman spectroscopy (Wei et al., 2018). The drilling and production testing in well SH-SC4 also confirmed the stratified coexistence of high saturation gas hydrates and water above BSR1; low saturation gas hydrate +free gas + water and free gas + water beneath BSR1 (Li et al., 2018; Qin et al., 2020). According to the gas hydrate phase equilibrium simulation (Figure 12B), the BGHSZ of the SI gas hydrates (BGHSI) was calculated using 100% methane and the *in situ* measured geothermal gradient in well SH-W04 at 229 mbsf, which is consistent with the depth of the seismically observed BSR1 (230 mbsf). The BGHSZ of the SII gas hydrate (BGHSII) was calculated using a gas composition of 99%C1 + 1%C2 at 240 mbsf, and the BGHSII was calculated using a gas composition of 98%C1 + 2%C2 at 310 mbsf. Both simulation results are inconsistent with the depth of BSR2 (320 mbsf) identified on the seismic profile. In addition, according to the gas composition of the hydrate-bound gas in this borehole (Table 1), a minor amount of ethane (1966–8430 ppm) was detected in the recovered hydrate-bound gas, which cannot form SII gas hydrate; therefore, the interpreted BSR2 may not be caused by the accumulation of SII gas hydrates formed by C2+ gas. Based on the above discussion, the coexistence of gas hydrates and free gas in the HGGHR reflects a dynamic gas hydrate system that may be the result of the active mud diapir and accompanying geothermal fluids, which destabilized the GHSZ and partially disassociated the gas hydrates to release free gas. The recycling of free gas between the double BSRs may have occurred in the HGGHR, which likely increased the gas hydrate saturation in the vicinity of BSR1 (Haacke et al., 2007; Yang and Davies, 2013; Nole et al., 2018; You et al., 2019). Over time, the free gas was continuously recycled into the GHSZ, increasing the thickness of the enriched gas hydrate-bearing layer. The above equilibrium calculations and the drilling and logging results for the HGGHR indicate that the double BSRs were formed due to a shift of the BGHSZ, which was likely caused by the ascent of geothermal fluids. In addition, the interval between the double BSRs may be the disequilibrium zone of the coexistence of gas hydrates and free gas, and dynamic recycling of gas hydrates and methane gas may have occurred, which contributed to the formation of the HGGHR in the study area.

5.2 Late transformation and preservation of the HGGHR

5.2.1 Faults in the GHSZ control the distribution of the gas hydrates and free gas

Multiple co-directional gliding faults were identified in the GHSZ of the trial production HGGHR from high-resolution 3-D seismic data and geoVISION logging data (Figures 4, 8). As the seismic profile and extracted attribute profile show (Figures 2-5), the faults generally cut the DBSRs in the gas hydrate-bearing layer and free gas-bearing layer. BSR1 and BSR2 are misaligned at the fault, showing a discontinuity. If the gas hydrates accumulated after the faults formed, then the BSR would be continuous. From the perspective of the time sequence, the gliding faults in the GHSZ are post-gas hydrate faults. In addition, the thickness of the gas hydrate-bearing layer is different in the hanging wall and footwall of the fault. If the fault existed before the formation of the gas hydrates, the thickness of the gas hydrate-bearing layer would be roughly the same in both walls of the fault. Therefore, the faults formed after the accumulation of the gas hydrate-bearing layers. Although the fault displacement is generally small, it could also shift the BGHSZ and may have had a significant influence on the later transformation of the gas hydrate reservoirs, resulting in the variations in the thickness and distribution of the gas hydrate-bearing layer and free gas-bearing layer in both walls of the fault (Yang and Davies, 2013). The seismic interpretation, LWD, and coring results have confirmed that the thickness of the gas hydrate-bearing layer is significantly thinner in the hanging wall of the fault than in the footwall of the fault (Figures 4, 7). Therefore, these post-gas hydrate faults developed in the GHSZ had a significant influence on the formation, accumulation, and distribution of the gas hydrates and associated free gas within the trail production HGGHR. In addition, a number of relatively larger gliding faults were identified on both sides of the gas hydrate reservoir, extending vertically upwards almost to the seafloor. The dissociated methane gas may have achieved submarine escape through these faults. Obviously, the distribution of the faults developed in the vicinity of the GHSZ ultimately controlled the outer boundary of the trail production HGGHR.

5.2.2 Preservation of the trial production HGGHR

Once most of the group-III gliding faults had cut the BSRs and deformed the sediments within the GHSZ, the sediments slide downward along the faults, which caused the variation in the phase equilibrium of the gas hydrates precipitated in the hanging wall and led to decomposition of the gas hydrates and the release of free gas. Since BSR1 overlies unconsolidated silty clay and clayey silt sediments that are characterized by a high porosity and thus lack an effective sealing ability, part of the free gas migrated upward along the fault and dissipation led to a decrease in the gas concentration. This resulted in a decrease in the thickness of the gas hydrate-bearing layer in the hanging wall of the gliding fault and a decrease in the gas hydrate saturation, while the phase equilibrium of the gas hydrates precipitated in the footwall may not have changed. When the fault activity stopped and the new phase equilibrium was reached, the thickness and saturation of the accumulated gas hydrates in the footwall of the current fault were relatively larger than those of gas hydrates in the hanging wall. After the new equilibrium was achieved and reaccumulation of the gas hydrates occurred, most of the recycled free gas was trapped and accumulated beneath BSR1 due to the self-sealing effect of the overlying gas hydrate-bearing sediments, resulting in a large range of acoustic chaotic reflections beneath BSR1 (Figure 4). The gas hydrate-bearing sediments in the Shenhu area are dominated by clayey silt or silty clay with a very fine grain size. A decrease in the grain size of a porous medium will reduce the sediment's permeability. In addition, the permeability of the gas hydrate-bearing deposits decreases exponentially with increasing gas hydrate saturation. The occurrence of late gliding faults will have a negative effect on the trail production gas hydrate accumulation and will lead to decomposition of the gas hydrates and possibly escape of the released free gas (Yang and Davies, 2013), in which situation, the low permeability strata will play a key role as a capping layer preventing the further migration of the released free gas. The low permeability sediment is conducive to the sealing and preservation of hydrocarbons entering the GHSZ and the recycling of the free gas released during gas hydrate dissociation, thus increasing the gas hydrate saturation in the HGGHR (Nole et al., 2018). Hence, the gliding faults developed in the GHSZ have an important influence on the distribution of the gas hydrates and free gas in the HGGHR. Based on the above discussion, we concluded that the group-III faults control the final distribution, scale, and reserves of the trial production gas hydrate reservoir. Although none active cold seep has been found in the Shenhu area at present, paleo-cold seeps as evidenced by geophysical, pore-water and authigenic sediment geochemistry have been reported by previous researchers (Lin et al., 2016; Deng et al., 2020; Hu et al., 2020; Liang et al., 2021; Zhang et al., 2022), indicating the post dissociation of gas hydrate and hydrocarbon seepage in the Shenhu area. Therefore, the preservation conditions of dynamic gas hydrate systems may act as determinants of the formation and distribution of the HGGHR.

5.3 Dynamic formation and accumulation model of the HGGHR

Based on the above discussion and taking the tectonic and sedimentary evolution and focused fluid flow history in the Shenhu area into consideration (Chen et al., 2013; Cheng et al., 2020; Zhang et al., 2021), we found that the formation and accumulation of the HGGHR in the Shenhu area has gone through a dynamic process under the influence of a deep mud diapir and an associated fault system, which can be summarized into three stages as follows (Figure 13). (1) Stage I was the initial stage of formation of the HGGHR. In the latest Miocene, the Dongsha Movement (~10 Ma) induced the release of overpressured fluid and the formation of the mud diapir and gas chimney in the Shenhu area (Chen et al., 2013). Under the hydrocarbon-rich generation background in the Baiyun Sag, the development of the mud diapir and associated group-I faults controlled the dual supply of deep thermogenic gas derived from the Paleogene source rocks and biogenic gas generated from the Miocene and overlying strata (Figures 2–4), creating a convex anticline-like feature and promoting the formation of a high saturation gas hydrate reservoir containing SI and SII gas hydrates and free gas (Figure 13A). (2) Stage II was the adjustment and recycling stage of the HGGHR. During the Miocene and Quaternary periods (~10 Ma–~2 Ma), due to the geothermal fluid activity of the diapir and possible increase of seabed temperature caused by the global warming, the temperature and pressure conditions of the originally formed gas hydrate reservoir changed and the BGHSZ shifted upward, resulting in decomposition of the gas hydrates and the release of free gas. In addition, with the development of the mud diapir the growing group-II faults extended into the GHSZ and continuously transported the released free gas upward. When the new equilibrium conditions were reached, the recycled free gas formed gas hydrates and accumulated again. The new BSR1 formed between the newly formed gas hydrate-bearing layer and the underlying gas hydrates and free gas. Part of BSR2 formed under the residual paleo-temperature and pressure conditions, and the superposed occurrence of gas hydrates, gas hydrates + free gas, and the free gas layer began to appear (Figure 13B). (3) Stage III was the transformation and preservation stage of the HGGHR. Since Quaternary (~2 Ma–Present), under the influence of the intensive thermal fluid activity of the diapir and the accompanying group-III faults and the erosion and filling of submarine channels in the shallow strata, the gas hydrates partially dissociated, leading to instability of the strata. When the gas hydrate-bearing sedimentary layer in the hanging wall of the fault slide downward, the gas hydrate phase equilibrium conditions changed and the gas hydrates continued to decompose. Due to the lack of an effective cap rock in the overlying layer, most of the free gas escaped and methane flow at seeps might have happened during this stage. The gas hydrate-bearing strata in the footwall were not affected, which eventually led to the thickness of the gas hydrate-bearing layer and free gas-bearing layer in the HGGHR being different in the hanging and footwalls (Figure 13C). In summary, under the conditions of a sufficient gas supply and the effective transportation via the mud diapir and diapir-associated fault system, the HGGHR was primarily altered by geothermal fluids and the gliding faults developed in the late stage, which finally controlled the accumulation of the gas hydrates above BSR1 and underlying coexistence of gas hydrate and free gas in the current HGGHR.

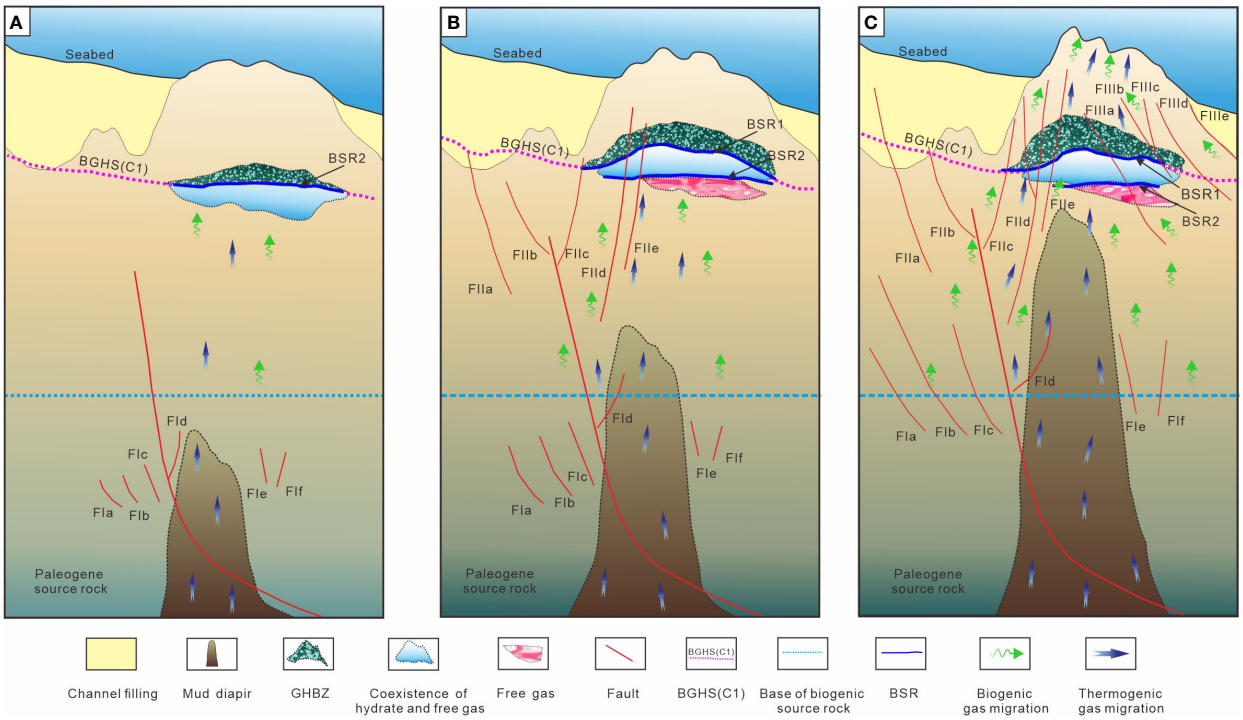

FIGURE 13
Dynamic migration and accumulation model of the trial production gas hydrate reservoir in the Shenhu area. **(A)** Stage I: Gas hydrate formation stage, **(B)** Stage II: gas hydrate adjustment stage, **(C)** Stage III: gas hydrate transformation and preservation stage. GHSZ: Gas hydrate stability zone. BGHSC1: Base of gas hydrate stability zone of 100% CH_4. GHBZ: Gas hydrate bearing zone.

6 Implications

Major breakthroughs have been made in gas hydrate production in areas with HGGHRs (Li et al., 2018; Yamamoto et al., 2019; Ye et al., 2020), which are the most ideal exploration target at present. Under the trend of global integration of gas hydrate exploration and development, the discovery of HGGHRs is the most urgent requirement for sustainable trial production and future efficient development. However, the study of the differential accumulation mechanism of HGGHRs is a key prerequisite for exploration and optimization of trial production and development targets. Two gas hydrate trial production breakthroughs in the SCS have further proven that a clayey silt-dominated gas hydrate reservoir can be efficiently mined despite its low permeability. Under the condition of the coexistence of recycled free gas and gas hydrates in a gas hydrate system, the effective step-down mining method is scientific and reasonable (Li et al., 2018; Ye et al., 2020). However, the coexistence of SI and SII gas hydrates poses a challenge in future gas hydrate production from below BSR1, because SII gas hydrates are more stable than SI gas hydrates. Therefore, the production conditions for controlling depressurization mining and secondary gas hydrate formation in a gas hydrate reservoir similar to the HGGHR in the Shenhu area should be addressed. In addition, the coupling relationship between the deep petroleum system and shallow gas hydrate system as well as evaluation of the contribution of gas-bearing fluid activity and free gas migration into gas hydrate reservoirs needs to be emphasized (Grauls, 2001). Structural characterization of the GHSZ and study of the temporal relationship between the formation and later reformation of gas hydrate reservoirs and tectonic and sedimentary events such as faults, gas chimneys, diapirs, and landslides are also important for understanding the accumulation mechanism of HGGHRs, as has been demonstrated by previous researches in the Qiongdongnan Basin near Shenhu area (Kuang et al., 2023), the Gulf of Mexico (Portnov et al., 2020), the Krishna-Godavari Basin offshore India (Riedel et al., 2010), the Opouawe Bank, New Zealand (Riedel et al., 2018), and the Danube Fan, Black Sea (Hillman et al., 2018b). Most importantly, the dynamic accumulation, late transformation, and preservation conditions of a gas hydrate system are also key points in exploring HGGHRs and optimizing the target of future trial production and the commercial development of gas hydrates.

7 Conclusions

The HGGHR is an ideal target for gas hydrate production. Based on high-resolution 3-D seismic data, LWD, coring, and testing, our understanding of the dynamic accumulation and late preservation of the trial production HGGHR in the Shenhu area were improved. The dual supply of biogenic gas and thermogenic gas was the basis for the precipitation and maintenance of the trial production HGGHR. Three types of newly identified multiple-stage faults associated with the development of the mud diapir beneath the HGGHR not only facilitated the migration of deep hydrate gas

but also shifted the BGHSZ due to its associated geothermal fluids, resulting in the dissociation of the gas hydrates and the release of free gas, as well as alteration of the double BSRs that were originally formed under different equilibrium conditions. The interval between the double BSRs should be a disequilibrium zone, and a gas recycling process occurs, which contributed to the coexistence of gas hydrates and free gas and the dynamic formation of the HGGHR. The HGGHR was reconstructed by the late gliding faults developed in the GHSZ, which also resulted in a shift in the BGHSZ and dynamic accumulation and adjustment of the gas hydrate-bearing layers and free gas-bearing layers within the HGGHR. The late transformation and preservation conditions of the gas hydrate system are important to the dynamic formation and accumulation of the HGGHR, which should be given serious consideration in future exploration and exploitation activities.

Data availability statement

The original contributions presented in the study are included in the article/Supplementary Material. Further inquiries can be directed to the corresponding authors.

Author contributions

WZ: Conceptualization, Funding acquisition, Resources, Writing – original draft, Writing – review & editing, Formal analysis, Investigation, Validation. JL: Conceptualization, Investigation, Project administration, Supervision, Data curation, Formal analysis, Funding acquisition, Methodology, Resources, Software, Validation, Visualization, Writing – review & editing. PS: Investigation, Project administration, Resources, Writing – review & editing. MM: Writing – review & editing, Data curation, Investigation, Resources. WH: Formal analysis, Software, Writing – review & editing, Investigation, Methodology. PL: Writing – review & editing. SY: Data curation, Formal analysis, Software, Validation, Writing – review & editing. CJ: Formal analysis, Software, Writing – review & editing, Data curation.

Funding

The author(s) declare that financial support was received for the research, authorship, and/or publication of this article. This work was supported by National Natural Science Foundation of China (42176215; 42076054). Project of Sanya Yazhou Bay Science and Technology City (SCKJ-JYRC-2023-02). Guangzhou Science and Technology Planning Project (202201011434). First Batch of "Nanhai New Star" project (NHXXRCXM202357). Sanya Science and Technology Innovation Project (2022KJCX14). National Key R&D Program of China (2018YFE0208200). National Engineering Research Center of Gas Hydrate Exploration and Development (NERC2024002). Open Found of Key Laboratory of Tectonics and Petroleum Resources (China University of Geosciences), Ministry of Education (No. TPR-2020-06).

Acknowledgments

We are grateful to reviewers and editors for their helpful suggestions and constructive comments that greatly improved this manuscript.

Conflict of interest

The authors declare that the research was conducted in the absence of any commercial or financial relationships that could be construed as a potential conflict of interest.

Publisher's note

References

Akihisa, B. B., Tezuka, K., Senoh, O., and Uchida, T. (2002). "Well log evaluation of gas hydrate saturation in the Miti Nankai-Trough well, offshore south east Japan," in *SPWLA 43rd Annual Logging Symposium* (Oiso, Japan: OnePetro).

Auguy, C., Calvès, G., Calderon, Y., and Brusset, S. (2017). Seismic evidence of gas hydrates, multiple bsrs and fluid flow offshore tumbes basin, Peru. *Mar. Geophys. Res.* 38, 409–423. doi: 10.1007/s11001-017-9319-2

Bohrmann, G., Greinert, J., Suess, E., and Torres, M. (1998). Authigenic carbonates from the Cascadia subduction zone and their relation to gas hydrate stability. *Geology* 26, 647–650. doi: 10.1130/0091-7613(1998)026<0647:ACFTCS>2.3.CO;2

Boswell, R., and Collett, T. (2006). The gas hydrates resource pyramid. *Natural Gas Oil* 304, 285–4541.

Boswell, R., Yoneda, J., and Waite, W. F. (2019). India National Gas Hydrate Program Expedition 02 summary of scientific results: Evaluation of natural gas-hydrate-bearing pressure cores. *Mar. Petroleum Geol.* 108, 143–153. doi: 10.1016/j.marpetgeo.2018.10.020

Bünz, S., Mienert, J., and Berndt, C. (2003). Geological controls on the storegga gas hydrate system of the mid-Norwegian continental margin. *Earth Planet. Sci. Lett.* 209, 291–307. doi: 10.1016/S0012-821X(03)00097-9

Bybee, K. (2004). Natural gas technology/monetization: overview of the mallik gas-hydrate production research well. *J. Pet. Technol.* 56, 53–54. doi: 10.2118/1004-0053-JPT

Chen, D. X., Wang, X., Völker, D., Wu, S., Wang, L., Li, W., et al. (2016). Three dimensional seismic studies of deep-water hazard-related features on the northern slope of South China Sea. *Mar. Petroleum Geol.* 77, 1125–1139. doi: 10.1016/j.marpetgeo.2016.08.012

Chen, D., Wu, S., Dong, D., Mi, L., Fu, S., and Shi, H. (2013). Focused fluid flow in the Baiyun Sag, northern South China Sea: implications for the source of gas in hydrate reservoirs. *Chin J Oceanol Limnol.* 31(1), 178–189.

Chen, F., Zhou, Y., Su, X., Liu, G. H., Lu, H. F., and Wang, J. L. (2011). Gas hydrate saturation and its relation with grain size of the hydrate-bearing sediments in the

Shenhu Area of northern South China Sea. *Mar. Geol. Quaternary Geol.* 31, 95–100. doi: 10.3724/SP.J.1140.2011.05095

Cheng, C., Jiang, T., Kuang, Z., Yang, C., Zhang, C., He, Y., et al. (2020). Characteristics of gas chimneys and their implications on gas hydrate accumulation in the Shenhu area, northern South China Sea. *J. Natural Gas Sci. Eng.* 84, 103629. doi: 10.1016/j.jngse.2020.103629

Chow, J., Lee, J. S., Sun, R., Liu, C. S., and Lundberg, N. (2000). Characteristics of the bottom simulating reflectors near mud diapirs: offshore southwestern Taiwan. *Geo-Marine Lett.* 20, 3–9. doi: 10.1007/s003670000034

Collett, T. S. (2000). "Natural gas hydrate as a potential energy resource," in *Natural Gas Hydrate* (Springer, Dordrecht), 123–136.

Collett, T. S. (2005). Results at Mallik highlight progress in gas hydrate energy resource research and development. *Petrophysics* 46, 237–243.

Collett, T. S. (2009). "Gas hydrate petroleum systems in marine and arctic permafrost environments", in *Unconventional Energy Resources: Making the Unconventional Conventional*. GCSSEPM Proc. doi: 10.5724/gcs.09.29.0006

Collett, T. S. (2013). "Gas hydrate reservoir properties," in *Unconventional Resources Technology Conference*. 1929–1937 (Denver, Colorado: Society of Exploration Geophysicists, American Association of Petroleum Geologists, Society of Petroleum Engineers).

Collett, T. S., Boswell, R., Waite, W. F., Kumar, P., Roy, S. K., Chopra, K., et al. (2019). India National Gas Hydrate Program Expedition 02 summary of scientific results: gas hydrate systems along the eastern continental margin of India. *Mar. Petroleum Geol.* 108, 39–142. doi: 10.1016/j.marpetgeo.2019.05.023

Collett, T. S., Johnson, A. H., Knapp, C. C., and Boswell, R. (2009). Natural gas hydrates-Energy resource potential and associated geologic hazard. *AAPG Memoir 89* 29, 858–869. doi: 10.1306/M891320

Collett, T. S., Lee, M. W., Agena, W. F., Miller, J. J., Lewis, K. A., Zyrianova, M. V., et al. (2011). Permafrost-associated natural gas hydrate occurrences on the Alaska North Slope. *Mar. Petroleum Geol.* 28, 279–294. doi: 10.1016/j.marpetgeo.2009.12.001

Crutchley, G. J., Klaeschen, D., Planert, L., Bialas, J., Berndt, C., Papenberg, C., et al. (2014). The impact of fluid advection on gas hydrate stability: Investigations at sites of methane seepage offshore Costa Rica. *Earth Planet. Sci. Lett.* 401, 95–109. doi: 10.1016/j.epsl.2014.05.045

Dallimore, S. R., and Collett, T. S. (2005). Scientific results from the mallik 2002 gas hydrate production research well program, mackenzie delta, northwest territories, Canada. *Bull. Geol. Survey Canada* 585, 957. doi: 10.4095/220702

Deng, Y., Chen, F., Hu, Y., Guo, Q., Cao, J., Chen, H., et al. (2020). Methane seepage patterns during the middle Pleistocene inferred from molybdenum enrichments of seep carbonates in the South China Sea. *Ore Geol. Rev.* 125, 103701. doi: 10.1016/j.oregeorev.2020.103701

Feseker, T., Pape, T., Wallmann, K., Klapp, S. A., Schmidt-Schierhorn, F., and Bohrmann, G. (2009). The thermal structure of the Dvurechenskii mud volcano and its implications for gas hydrate stability and eruption dynamics. *Mar. Petroleum Geol.* 26, 1812–1823. doi: 10.1016/j.marpetgeo.2009.01.021

Fujii, T., Suzuki, K., Takayama, T., Tamaki, M., Komatsu, Y., Konno, Y., et al. (2015). Geological setting and characterization of a methane hydrate reservoir distributed at the first offshore production test site on the Daini-Atsumi Knoll in the eastern Nankai Trough, Japan. *Mar. Petroleum Geol.* 66, 310–322. doi: 10.1016/j.marpetgeo.2015.02.037

Grauls, D. (2001). Gas hydrates: importance and applications in petroleum exploration. *Mar. Petroleum Geol.* 18, 519–523. doi: 10.1016/S0264-8172(00)00075-1

Haacke, R. R., Westbrook, G. K., and Hyndman, R. D. (2007). Gas hydrate, fluid flow and free gas: Formation of the bottom-simulating reflector. *Earth Planet. Sci. Lett.* 261, 407–420. doi: 10.1016/j.epsl.2007.07.008

Han, S., Bangs, N. L., Hornbach, M. J., Pecher, I. A., Tobin, H. J., and Silver, E. A. (2021). The many double BSRs across the northern Hikurangi margin and their implications for subduction processes. *Earth Planet. Sci. Lett.* 558, 116743. doi: 10.1016/j.epsl.2021.116743

Herron, M. M. (1987). *Estimationg the intrinsic permeability of classic sediments from geochemical data[C]//SPWLA 28th Annual Symposium* (London, England), 200–223.

Hillman, J. I., Burwicz, E., Zander, T., Bialas, J., Klaucke, I., Feldman, H., et al. (2018a). Investigating a gas hydrate system in apparent disequilibrium in the Danube Fan, Black Sea. *Earth Planet. Sci. Lett.* 502, 1–11. doi: 10.1016/j.epsl.2018.08.051

Hillman, J. I., Klaucke, I., Bialas, J., Feldman, H., Drexler, T., Awwiller, D., et al. (2018b). Gas migration pathways and slope failures in the Danube Fan, Black Sea. *Mar. Petroleum Geol.* 92, 1069–1084. doi: 10.1016/j.marpetgeo.2018.03.025

Hsu, H., Liu, C., Chang, Y., Chang, J., Ko, C., Chiu, S., et al. (2017). Diapiric activities and intraslope basin development offshore of SW Taiwan: A case study of the Lower Fangliao Basin gas hydrate prospect. *J. Asian Earth Sci.* 149, 145–159. doi: 10.1016/j.jseaes.2017.05.007

Hu, Y., Feng, D., Peckmann, J., Gong, S., Liang, Q., Wang, H., et al. (2020). The impact of diffusive transport of methane on pore-water and sediment geochemistry constrained by authigenic enrichments of carbon, sulfur, and trace elements: a case study from the Shenhu area of the South China Sea. *Chem. Geol.* 553, 119805. doi: 10.1016/j.chemgeo.2020.119805

Jang, J., Waite, W. F., Stern, L. A., Collett, T. S., and Kumar, P. (2019). Physical property characteristics of gas hydrate-bearing reservoir and associated seal sediments collected during NGHP-02 in the Krishna-Godavari Basin, in the offshore of India. *Mar. Petroleum Geol.* 108, 249–271. doi: 10.1016/j.marpetgeo.2018.09.027

Kim, K. J., Yi, B. Y., Kang, N. K., and Yoo, D. G. (2015). Seismic attribute analysis of the indicator for gas hydrate occurrence in the northwest Ulleung Basin, East Sea. *Energy Proc.* 76, 463–469. doi: 10.1016/j.egypro.2015.07.882

Konno, Y., Fujii, T., Sato, A., Akamine, K., Naiki, M., Masuda, Y., et al. (2017). Key findings of the world's first offshore methane hydrate production test off the coast of Japan: Toward future commercial production. *Energy Fuels* 31, 2607–2616. doi: 10.1021/acs.energyfuels.6b03143

Kuang, Z., Cook, A., Ren, J., Deng, W., Cao, Y., and Cai, H. (2023). A flat-lying transitional free gas to gas hydrate system in a sand layer in the Qiongdongnan Basin of the South China Sea. *Geophys. Res. Lett.* 50, e2023GL105744. doi: 10.1029/2023GL105744

Kunath, P., Chi, W. C., Berndt, C., Chen, L., Liu, C. S. , Kläschen, D., et al. (2020). A shallow seabed dynamic gas hydrate system off SW Taiwan: Results from 3-D seismic, thermal, and fluid migration analyses. *J. Geophys. Res.: Solid Earth* 125, e2019JB019245-T. doi: 10.1029/2019JB019245

Li, J., Lu, J., Ning, F., Lu, H., and Liang, J. (2019). Lithological characteristics and hydrocarbon gas sources of gas hydrate-bearing sediments in the shenhu area, South China Sea: implications from the sc-w01b and sc-w02b sites. *Mar. Geol.* 408, 36–47. doi: 10.1016/j.margeo.2018.10.013

Li, J. F., Ye, J. L., Qin, H. J., Wu, N. Y., Lu, H. L., Xie, W. W., et al. (2018). The first offshore natural gas hydrate production test in the South China Sea. *China Geol.* 1, 5–16. doi: 10.31035/cg2018003

Liang, Q., Xiao, X., Zhao, J., Zhang, W., Li, Y., Wu, X., et al. (2022). Geochemistry and sources of hydrate-bound gas in the Shenhu area, northern South China Sea: Insights from drilling and gas hydrate production tests. *J. Petroleum Sci. Eng.* 208, 109459. doi: 10.1016/j.petrol.2021.109459

Liang, J., Zhang, Z., Lu, J., Guo, Y., Sha, Z., Su, P., et al. (2021). Characterization of gas accumulation at a venting gas hydrate system in the Shenhu area, South China Sea. *Interpretation* 9(2), SD1–SD14.

Liang, J. Q., Zhang, W., Lu, J. A., Wei, J. G., Kuang, Z. G., He, Y. L., et al. (2019). Geological occurrence and accumulation mechanism of natural gas hydrates in the eastern Qiongdongnan Basin of the South China Sea: Insights from site GMGS5-W9–2018. *Mar. Geol.* 418, 106042. doi: 10.1016/j.margeo.2019.106042

Liang, J., Zhang, Z., Su, P., Sha, Z., and Yang, S. (2017). Evaluation of gas hydrate-bearing sediments below the conventional bottom-simulating reflection on the northern slope of the South China Sea. *Interpretation* 5, SM61–SM74. doi: 10.1190/INT-2016-0219.1

Lin, Z., Sun, X., Lu, Y., Xu, L., Gong, J., Lu, H., et al. (2016). Stable isotope patterns of coexisting pyrite and gypsum indicating variable methane flow at a seep site of the Shenhu area, South China Sea. *J. Asian Earth Sci.* 123, 213–223. doi: 10.1016/j.jseaes.2016.04.007

Liu, J. W., and Li, X. S. (2021). Recent advances on natural gas hydrate exploration and development in the South China Sea. *Energy Fuels* 35, 7528–7552. doi: 10.1021/acs.energyfuels.1c00494

Lu, Z., Zhu, Y., Liu, H., Zhang, Y., Jin, C., Huang, X., et al. (2013). Gas source for gas hydrate and its significance in the Qilian Mountain permafrost, Qinghai. *Mar. Petroleum Geol.* 43, 341–348. doi: 10.1016/j.marpetgeo.2013.01.003

Lüdmann, T., and Wong, H. (2003). Characteristics of gas hydrate occurrences associated with mud diapirism and gas escape structures in the northwestern Sea of Okhotsk. *Mar. Geol.* 201, 269–286. doi: 10.1016/S0025-3227(03)00224-X

Makogon, Y. F., Holditch, S. A., and Makogon, T. Y. (2007). Natural gas-hydrates—A potential energy source for the 21st Century. *J. Petroleum Sci. Eng.* 56, 14–31. doi: 10.1016/j.petrol.2005.10.009

Ning, X., Shiguo, W., Buqing, S., Bing, L., Liangqing, X., Xiujuan, W., et al. (2009). Gas hydrate associated with mud diapirs in southern Okinawa Trough. *Mar. Petroleum Geol.* 26, 1413–1418. doi: 10.1016/j.marpetgeo.2008.10.001

Nole, M., Daigle, H., Cook, A. E., Malinverno, A., and Flemings, P. B. (2018). Burial-driven methane recycling in marine gas hydrate systems. *Earth Planet. Sci. Lett.* 499, 197–204. doi: 10.1016/j.epsl.2018.07.036

Paganoni, M., Cartwright, J. A., Foschi, M., Shipp, C. R., and Rensbergen, P. V. (2016). Structure II gas hydrates found below the bottom-simulating reflector. *Geophys. Res. Lett.* 43, 5696–5706. doi: 10.1002/2016GL069452

Pang, X., Chen, C., Chen, H., He, M., Shen, J., Liu, B., et al. (2008). A study on hydrocarbon accumulation dynamics in Baiyun deep-water area, Pearl River Mouth basin. *China Offshore Oil Gas* 20, 9–14. in Chinese with English abstract.

Portnov, A., Cook, A. E., Heidari, M., Sawyer, D. E., Santra, M., and Nikolinakou, M. (2020). Salt-driven evolution of a gas hydrate reservoir in Green Canyon, Gulf of Mexico. *AAPG Bull.* 104, 1903–1919. doi: 10.1306/10151818125

Portnov, A., You, K., Flemings, P., Cook, A., Heidari, M., Sawyer, D., et al. (2023). Dating submarine landslides using the transient response of gas hydrate stability. *Geology* 51, 387–391. doi: 10.1130/G50930.1

Qian, J., Wang, X., Collett, T. S., Guo, Y., Kang, D., and Jin, J. (2018). Downhole log evidence for the coexistence of structure II gas hydrate and free gas below the bottom simulating reflector in the South China Sea. *Mar. Petroleum Geol.* 98, 662–674. doi: 10.1016/j.marpetgeo.2018.09.024

Qin, X. W., Lu, J. A., Lu, H. L., Qiu, H. J., Liang, J. Q., Kang, D. J., et al. (2020). Coexistence of natural gas hydrate, free gas and water in the gas hydrate system in the Shenhu Area, South China Sea. *China Geol.* 3, 210–220. doi: 10.31035/cg2020038

Riedel, M., Collett, T. S., Kumar, P., Sathe, A. V., and Cook, A. (2010). Seismic imaging of a fractured gas hydrate system in the Krishna–Godavari Basin offshore India. *Mar. Petroleum Geol.* 27, 1476–1493. doi: 10.1016/j.marpetgeo.2010.06.002

Riedel, M., Crutchley, G., Koch, S., Berndt, C., Bialas, J., Eisenberg-Klein, G., et al. (2018). Elongate fluid flow structures: Stress control on gas migration at Opouawe Bank, New Zealand. *Mar. Petroleum Geol.* 92, 913–931. doi: 10.1016/j.marpetgeo.2018.03.029

Riedel, M., Freudenthal, T., Bialas, J., Papenberg, C., Haeckel, M., Bergenthal, M., et al. (2021). *In-situ* borehole temperature measurements confirm dynamics of the gas hydrate stability zone at the upper Danube deep sea fan, Black Sea. *Earth Planet. Sci. Lett.* 563, 116869. doi: 10.1016/j.epsl.2021.116869

Shao, L., Pang, X., Qiao, P., Chen, C., Li, Q., and Miao, W. (2008). Sedimentary filling of the Pearl River Mouth Basin and its response to the evolution of the Pearl River. *Acta Sedimentol Sin.* 26, 179.

Shukla, K. M., Collett, T. S., Kumar, P., Yadav, U. S., Boswell, R., Frye, M., et al. (2019). National gas hydrate program expedition 02: Identification of gas hydrate prospects in the Krishna-Godavari Basin, offshore India. *Mar. Petroleum Geol.* 108, 167–184. doi: 10.1016/j.marpetgeo.2018.11.013

Sloan, E. D. (1998). Clathrate hydrates of natural gas. *Marced Dekker New York*, 726.

Smith, A. J., Flemings, P. B., Liu, X., and Darnell, K. (2014). The evolution of methane vents that pierce the hydrate stability zone in the world's oceans. *J. Geophys. Res.: Solid Earth* 119, 6337–6356. doi: 10.1002/2013JB010686

Su, P., Liang, J., Peng, J., Zhang, W., and Xu, J. (2018). Petroleum systems modeling on gas hydrate of the first experimental exploitation region in the Shenhu area, northern South China Sea. *J. Asian Earth Sci.* 168, 57–76. doi: 10.1016/j.jseaes.2018.08.001

Su, P., Liang, J., Qiu, H., Xu, J., Ma, F., Li, T., et al. (2023). Quantitative simulation of gas hydrate formation and accumulation with 3d petroleum system modeling in the Shenhu area, northern South China Sea. *Energies* 16, 99. doi: 10.3390/en16010099

Su, M., Sha, Z., Zhang, C., Wang, H., Wu, N., Yang, R., et al. (2017). Types, characteristics and significances of migrating pathways of gasbearing fluids in the Shenhu area, northern continental slope of the South China Sea. *Acta Geol. Sinica (English Edition)* 91, 219–231. doi: 10.1111/1755-6724.13073

Su, M., Yang, R., Wang, H. B., Sha, Z. B., Liang, J. Q., and Wu, N. Y. (2016). Gas hydrates distribution in the Shenhu Area, northern South China Sea: comparisons between the eight drilling sites with gas-hydrate petroleum system. *Geol. Acta* 14, 79–100. doi: 10.1344/GeologicaActa2016.14.2.1

Timur, A. (1969). Producible porosity and permeability of sandstone investigated through Nuclear Magnetic Resonance principles. *Log Analyst* 10, 3–11.

Wan, Z., Xu, X., Wang, X., Xia, B., and Sun, Y. (2017). Geothermal analysis of boreholes in the Shenhu gas hydrate drilling area, northern South China Sea: Influence of mud diapirs on hydrate occurrence. *J. Petroleum Sci. Eng.* 158, 424–432. doi: 10.1016/j.petrol.2017.08.053

Wang, X., Collett, T. S., Lee, M. W., Yang, S. X., Guo, Y. Q., and Wu, S. G. (2014). Geological controls on the occurrence of gas hydrate from core, downhole log, and seismic data in the Shenhu area, South China Sea. *Mar. Geol.* 357, 272–292. doi: 10.1016/j.margeo.2014.09.040

Wang, J., Wu, S., and Yao, Y. (2018). Quantifying gas hydrate from microbial methane in the South China Sea. *J. Asian Earth Sci.* 168, 48–56. doi: 10.1016/j.jseaes.2018.01.020

Wei, J., Fang, Y., Lu, H., Lu, H., Lu, J., Liang, J., et al. (2018). Distribution and characteristics of natural gas hydrates in the Shenhu Sea Area, South China Sea. *Mar. Petroleum Geol.* 98, 622–628. doi: 10.1016/j.marpetgeo.2018.07.028

Wu, Q., Jiang, G., and Zhang, P. (2010). Assessing the permafrost temperature and thickness conditions favorable for the occurrence of gas hydrate in the Qinghai–Tibet Plateau. *Energy Conversion Manage.* 51, 783–787. doi: 10.1016/j.enconman.2009.10.035

Xie, H., Zhou, D., Pang, X., Li, Y., Wu, X., Qiu, N., et al. (2013). Cenozoic sedimentary evolution of deepwater sags in the Pearl River Mouth Basin, northern South China Sea. *Mar. Geophys. Res.* 34, 159–173. doi: 10.1007/s11001-013-9183-7

Yamamoto, K., Wang, X. X., Tamaki, M., and Suzuki, K. (2019). The second offshore production of methane hydrate in the Nankai Trough and gas production behavior from a heterogeneous methane hydrate reservoir. *RSC Adv.* 9, 25987–26013. doi: 10.1039/C9RA00755E

Yang, J., and Davies, R. J. (2013). Gravity-driven faults: Migration pathways for recycling gas after the dissociation of marine gas hydrates. *Mar. Geol.* 336, 1–9. doi: 10.1016/j.margeo.2012.11.013

Yang, S. X., Lei, Y., Liang, J. Q., Holland, M., Schultheiss, P., Lu, J. A., et al. (2017). "Concentrated gas hydrate in the Shenhu Area, South China Sea: Results from drilling expeditions GMGS3 & GMGS4," in *Proceedings of 9th International Conference on Gas Hydrates*. 25–30.

Yang, S., Liang, J., Lu, J., Qu, C., and Liu, B. (2017). New understandings on the characteristics and controlling factors of gas hydrate reservoirs in the Shenhu area on the northern slope of the South China Sea. *Earth Sci. Front.* 24, 1–14. in Chinese with English abstract.

Ye, J., Qin, X., Qiu, H., Xie, W., Lu, H., Lu, C., et al. (2018). Data report: molecular and isotopic compositions of the extracted gas from China's first offshore natural gas hydrate production test in South China Sea. *Energies* 11, 2793. doi: 10.3390/en11102793

Ye, J., Qin, X., Xie, W., Lu, H., Ma, B., Qiu, H., et al. (2020). The second natural gas hydrate production test in the South China Sea. *China Geol.* 2, 197–209. doi: 10.31035/cg2020043

Ye, J., Wei, J., Liang, J., Lu, J., Lu, H., and Zhang, W. (2019). Complex gas hydrate system in a gas chimney, South China Sea. *Mar. Petroleum Geol.* 104, 29–39. doi: 10.1016/j.marpetgeo.2019.03.023

You, K., Flemings, P. B., Malinverno, A., Collett, T. S., and Darnell, K. (2019). Mechanisms of methane hydrate formation in geological systems. *Rev. Geophys.* 57, 1146–1196. doi: 10.1029/2018RG000638

Zander, T., Haeckel, M., Berndt, C., Chi, W., Klaucke, I., Bialas, J., et al. (2017). On the origin of multiple BSRs in the Danube deep- sea fan, Black Sea. *Earth Planet. Sci. Lett.* 462, 15–25. doi: 10.1016/j.epsl.2017.01.006

Zhang, G., Feng, C., Yao, X., Ji, M., Yang, H., Qu, H., et al. (2021). Petroleum geology in deepwater settings in a passive continental margin of a marginal sea: a case study from the South China Sea. *Acta Geol. Sinica-English Edition* 95, 1–20. doi: 10.1111/1755-6724.14621

Zhang, W., Liang, J. Q., Lu, J. A., Wei, J. G., Su, P. B., Fang, Y. X., et al. (2017). Accumulation features and mechanisms of high saturation natural gas hydrate in Shenhu area, northern South China Sea. *Petroleum Explor. Dev.* 44, 670–680. doi: 10.1016/S1876-3804(17)30082-4

Zhang, W., Liang, J., Wan, Z., Su, P., Huang, W., Wang, L., et al. (2020a). Dynamic accumulation of gas hydrates associated with the channel-levee system in the Shenhu area, northern South China Sea. *Mar. Petroleum Geol.* 117, 104354. doi: 10.1016/j.marpetgeo.2020.104354

Zhang, W., Liang, J., Wei, J., Su, P., Lin, L., and Huang, W. (2019). Origin of natural gases and associated gas hydrates in the Shenhu area, northern South China Sea: Results from the China gas hydrate drilling expeditions. *J. Asian Earth Sci.* 183, 103953. doi: 10.1016/j.jseaes.2019.103953

Zhang, W., Liang, J., Wei, J., Su, P., Lin, L., Huang, W., et al. (2020b). Geological and geophysical features of and controls on occurrence and accumulation of gas hydrates in the first offshore gas-hydrate production test region in the Shenhu area, Northern South China Sea. *Mar. Petroleum Geol.* 114, 104191. doi: 10.1016/j.marpetgeo.2019.104191

Zhang, G., Liang, J., Yang, S., Zhang, M., Holland, M., Schultheiss, P., et al. (2015). Geological features, controlling factors and potential prospects of the gas hydrate occurrence in the east part of the Pearl River Mouth Basin, South China Sea. *Mar. Petroleum Geol.* 67, 356–367. doi: 10.1016/j.marpetgeo.2015.05.021

Zhang, Z., and Wright, C. (2017). Quantitative interpretations and assessments of a fractured gas hydrate reservoir using three-dimensional seismic and LWD data in Kutei Basin, East Kalimantan, offshore Indonesia. *Mar. Petroleum Geol.* 84, 257–273. doi: 10.1016/j.marpetgeo.2017.03.019

Zhang, Q., Wu, D. ,. G., Xu, X., Yang, C., and Liu, L. (2022). Methane seep in the Shenhu area of the South China sea using geochemical and mineralogical features. *Mar. Petroleum Geol.* 144, 105829. doi: 10.1016/j.marpetgeo.2022.105829

Zhang, G., Yang, H., Chen, Y., JI, M., Wang, K., Yang, D., et al. (2014). The Baiyun Sag: A giant rich gas-generation sag in the deepwater area of the Pearl River Mouth Basin. *Natural Gas Industry* 34, 11–25. in Chinese with English abstract.